This article may be downloaded for personal use only. Any other use requires prior permission of the author and AIP Publishing. This article appeared in (citation of published article) and may be found at https://doi.org/10.1063/5.0188464
Postprint of: Bartłomiejczyk P., Trujillo F. L., Signerska-Rynkowska J., Analysis of dynamics of a map-based neuron model via Lorenz maps, CHAOS, Vol. 34 (2024), 043110

ANALYSIS OF DYNAMICS OF A MAP-BASED NEURON MODEL VIA LORENZ MAPS

PIOTR BARTŁOMIEJCZYK

Faculty of Applied Physics and Mathematics & BioTechMed Centre, Gdańsk University of Technology, Gabriela Narutowicza 11/12, 80-233 Gdańsk, Poland.
Email address: piobartl@pg.edu.pl; Orcid ID: 0000-0001-5779-4428

FRANK LLOVERA TRUJILLO

Doctoral School, Gdańsk University of Technology, Gabriela Narutowicza 11/12, 80-233 Gdańsk, Poland.
Email address: frank.llovera.trujillo@pg.edu.pl; Orcid ID: 0000-0001-5979-3584

JUSTYNA SIGNERSKA-RYNKOWSKA*

Faculty of Applied Physics and Mathematics & BioTechMed Centre, Gdańsk University of Technology, Gabriela Narutowicza 11/12, 80-233 Gdańsk, Poland;
Dioscuri Centre in Topological Data Analysis, Institute of Mathematics of the Polish Academy of Sciences, Śniadeckich 8, 00-656 Warsaw, Poland.
Email address: justyna.signerska@pg.edu.pl; Orcid ID: 0000-0002-9704-0425

Abstract. modelling nerve cells can facilitate formulating hypotheses about their real behaviour and improve understanding their functioning. In this paper we study a discrete neuron model introduced by Courbage, Nekorkin and Vdovin (*Chaos* 17, 043109, 2007). where the originally piecewise linear function defining voltage dynamics is replaced by a cubic polynomial, with an additional parameter responsible for varying the slope. Showing that on a large subset of the multidimensional parameter space the return map of the voltage dynamics is an expanding Lorenz map, we analyze both chaotic and periodic behaviour of the system and describe complexity of spiking patterns fired by a neuron. This is achieved by using and extending some results from the theory of Lorenz-like and expanding Lorenz mappings.

Map-based models form an important class of models describing the dynamics of a single nerve cell, which effectively complement earlier ODE-based ones. Although these models might seem abstract from the biological point of view, their electrophysiological relevance is in many cases more than satisfactory. Moreover, their relative low computational complexity enables to employ them successfully in larger scale simulations of neuronal circuits motivated by biological or clinical issues. However, prior to examination of large ensembles of coupled neurons, it is desirable to understand the dynamical mechanisms behind the phenomena observed in the chosen single neuron model. In 2007 Courbage, Nekorkin and Vdovin introduced a discrete neuron model where the membrane voltage dynamics was captured by the iterates of the piecewise linear discontinuous map. In this work we undertake a

Date: April 2, 2024.
2020 *Mathematics Subject Classification.* Primary: 37E05, 37E45, 37N25; Secondary: 37E15, 92C20.
Key words and phrases. neuronal dynamics, Lorenz-like maps, expanding Lorenz maps, chaos, Farey-Lorenz permutations, periodic spiking.
*Corresponding author.

rigorous study of its later version where, following the prominent FitzHugh-Nagumo model, the piecewise linear function is replaced by a cubic polynomial with a discontinuity point. In particular, using recent advances of the theory of Lorenz-like maps, we quantify chaotic behaviour and firing patterns displayed by a reduced CNV model.

Introduction

Modelling neuronal behaviour dates back to the beginning of previous century when Lapicque ([40]) formulated a simple neuron model, derived from experimental data. This model later gave rise to the famous leaky-integrate-and-fire (LIF) model (see e.g. [12]). A couple of decades later Hodgkin and Huxley derived a much more detailed neuron model ([29]), consisting of four nonlinear differential equations, that were able to capture many electrophysiological phenomena present in real neurons. Since this pioneering model, systems based on ODEs became a standard in modelling of biological neurons with some later prominent examples of FitzHugh–Nagumo [21, 49], Hindmarsh–Rose [28], Morris–Lecar [47] and other models. These models were usually significantly simpler than the original Hodgkin-Huxley model but served as a good toy models for explaining the mechanism of action potential generation and sometimes more complicated phenomena like *bursting* (a repetitive behaviour where a series of spikes occurs in a rapid succession followed by a quiescent period).

These lower dimensional reduced models have the advantage of enabling rigorous analysis but the continuous-time dynamics given by systems of ODEs requires often more dimensions or separation of time scales to capture more complicated phenomena. Therefore there appeared a need for some sort of discretization of these models. The first pronounced step in this direction was the appearance of hybrid neuron models, in which the interspike evolution of transmembrane voltage and other variables is governed by ODEs but the additional threshold-reset mechanism is introduced in order to better reproduce spikes generation. The hybrid nature makes these models interesting even in one dimensional setting ([9, 13, 16, 38]) but one dimensional integrate-and-fire (IF) models are too simple e.g. to display bursting behaviour. However, two-dimensional IF models ([10, 31, 62]) feature both bursting and other complicated phenomena such as e.g. spike-adding or mixed-mode oscillations ([56, 57]) that in ODE-systems need at least three dimensions and often separation of time-scales.

Another class of deterministic neuron models are so-called map-based models where differential equations are replaced by maps. These models might also involve some sort of resetting mechanism which is usually incorporated in the map describing the evolution of the membrane voltage. However, many map-based models do not include directly any kind of resetting mechanism. Instead, purely discrete nature of these models can give rise to very complicated phenomena, yet their computational feasibility allows for simulating large networks consisting of map-based neurons. Some of these models arise simply as discretization of ODE-based models, whereas others rather cannot be linked with any ODE system (see e.g. [30] for an extensive review on map-based models).

Most of the two-dimensional map based models can be expressed in a general form:

$$x_{n+1} = F(x_n, y_n), \tag{1a}$$

$$y_{n+1} = y_n + \varepsilon G(x_n, y_n), \tag{1b}$$

where often $0 < \varepsilon \ll 1$ to include separation of time scales. The main dynamical variable x stands for the membrane voltage and y is usually called *adaptation* or *recovery* variable, which replaces complicated dynamics of ion channels. Separation of time scales as $\varepsilon \to 0$ also justifies studying the first return map $x_{n+1} = F(x_n, y)$ as $y_n \equiv y$ is kept constant since this map governs the most important dynamical properties of (1a)-(1b). Similarly, this map allows to understand intuitively such phenomena like bursting and adaptation since y can be interpreted as a slowly varying bifurcation parameter in the map $F_y(x) := F(x, y)$ and the types of bifurcations governing

MOST WIEDZY Downloaded from mostwiedzy.pl

the onset and termination of limit cycles of map F are closely related to the classification of bursting patterns in a map-based models ([32]).

Popular 2D map-based (discrete) neuron models include e.g. Rulkov model ([58]), Chialvo model ([15]) or Courbage, Nekorkin and Vdovin model ([17]). The last one, called CNV for short, or precisely its modification, will be the subject of our study presented in this work. However, let us firstly briefly mention some other properties of the above listed models.

The *chaotic Rulkov model* ([58]) is given as

$$x_{n+1} = \frac{\alpha}{1+x_n^2} + y_n + I, \tag{2a}$$

$$y_{n+1} = y_n - \varepsilon(x_n - \sigma), \tag{2b}$$

where I describes external input or synaptic currents applied to the neuron and σ denotes the resting potential. In this model the function $F(x,y) := \frac{\alpha}{1+x^2} + y + I$ is a unimodal map as a function of x for fixed y. This map can feature a stable and unstable fixed points on the left branch, which disappear under saddle-node bifurcation as I increases. Initial conditions attracted to the stable fixed point correspond to the resting state of the model. On the other hand, spiking orbits are chaotic, not periodic, which is the important property of the model as irregular bursting is more similar to realistic bursting neurons than periodic bursting ([39]). In fact, chaotic dynamics in systems such as Rulkov model is robust and can be classified with some notion of regularity ([33]) which is actually consistent with physiological function of neurons. Note that there are also other versions of Rulkov model, called *non-chaotic Rulkov model* ([59]) and *supercritical Rulkov model* ([60]).

The *Chialvo model* ([15]) is given as

$$x_{n+1} = x_n^2 \exp(y_n - x_n) + I, \tag{3a}$$

$$y_{n+1} = a y_n - b x_n + c. \tag{3b}$$

It turns out that the map $F(x,y) := x^2 \exp(y-x) + I$ defining the evolution of the voltage variable is unimodal (for fixed y) on some invariant interval, similarly as Rulkov map. However, here its dependence on the recovery variable y is not additive, but non-linear and therefore a small change in the value of y changes the shape of the x-nullcline in a much more complicated way than in case of Rulkov map. Nevertheless, this model, designed as an excitable neuron model, also reveals chaotic spiking, periodic spiking, as well as bistability and subthreshold oscillations. More detailed analysis of its 1D subsystem $x_{n+1} = F(x_n, y)$ can be done upon noticing that the map F (again for fixed y) has negative Schwarzian derivative ([42]). Since the model does not follows exactly a typical form of slow-fast map based neuron models (1a)-(1b), its singular perturbation analysis also requires more general tools ([34]).

Although Chialvo model was introduced in 1995, there is again a growing interest in this model. This is particularly due to its dependence on many parameters and the fact that small variation in these parameters can significantly change its phase portrait. Therefore rigorous analysis of its global dynamics requires new computational and analytical tools ([53]). On the other hand, many extensions of this model also have emerged recently (see e.g. [61]). A more detailed discussion of various discrete neuron models and how they relate to ODE-based models can be found in review articles [18, 30].

In the current work we undertake the study of the following two-dimensional discrete neuron model:

$$x_{n+1} = f_1(x_n, y_n) = x_n + F(x_n) - y_n - \beta H(x_n - d), \tag{4a}$$

$$y_{n+1} = f_2(x_n, y_n) = y_n + \varepsilon(x_n - J), \tag{4b}$$

introduced by Courbage, Nekorkin and Vdovin ([17]) and further called the CNV model (for short). In this model, as before, x_n denotes the values of the membrane potential of the neuron at consecutive time instances $n = 1, 2 \ldots$ and y_n the values of the recovery variable. The function $H(x)$ is

MOST WIEDZY Downloaded from mostwiedzy.pl

the usual Heaviside step function:

$$H(x) = \begin{cases} 1, & \text{if } x \geq 0, \\ 0, & \text{if } x < 0. \end{cases}$$

Parameter $\varepsilon > 0$ describes the time scale separation between variables x and y, J might stand for a constant external stimulus whereas $\beta > 0$ and $d > 0$ control the threshold properties of oscillations. Typically, $F(x)$ is defined as follows:

$$F(x) = \begin{cases} -m_0 x, & \text{if } x \leq J_{\min}, \\ m_1(x-a), & \text{if } J_{\min} \leq x \leq J_{\max}, \\ -m_0(x-1), & \text{if } x \geq J_{\max}, \end{cases} \tag{5}$$

where

$$m_0, m_1 > 0, \quad 1 > a > 0, \quad J_{\min} = \frac{am_1}{m_0 + m_1}, \quad J_{\max} = \frac{m_0 + am_1}{m_0 + m_1}.$$

Due to the piecewise linear form of $F(x)$ the model (4a)-(4b) with F given by (5) will be referred to as the plCNV model (piecewise linear CNV model). Detailed analysis of this model, and especially its first return map, was performed in our recent paper [6]. However, given the similarity of the CNV model with FitzHugh-Nagumo one ([20, 21]), it seems natural to replace the piecewise linear function F with some cubic polynomial (see [18]). Of course, introducing a nonlinear function F requires a bit different analytical tools (in particular, the theory of β-transformations, successively applied in [6], must be replaced by the general theory of Lorenz-like or expanding Lorenz maps).

The CNV model displays a range of attractors and regimes of neural activity, including phasic spiking, phasic bursts, tonic spiking, chaotic spiking, subthreshold oscillations or chaotic bursting oscillations. General conditions in parameter spaces for these various types of qualitative behaviour have been identified in [17].

In this paper we study the CNV model, where the function F is defined as

$$F(x) = \mu x(x-a)(1-x), \tag{6}$$

with $\mu > 0$ and $0 < a < 1$. The model (4a)-(4b) where F is given by (6) will be called in our analysis nonlinear CNV model and denoted nlCNV. Its simplified one dimensional version consisting of (4a), with $y_n := \alpha$ being a constant parameter, will be referred to as the 1D nlCNV model.

Our study of the 1D nlCNV model is motivated, among others, by the fact that it actually governs the behaviour of the full model and thorough understanding of its properties such as chaos and structure of periodic orbits with respect to y and other parameters is essential. Obviously, this one dimensional system is also interesting from purely mathematical point of view. However, as 1D map based-models are also known in the literature (e.g. the models proposed by Aguirre et al. [1], Cazelles et al. [14] or just the fast subsystem of the chaotic Rulkov model, see the review articles [18, 30] and references therein), we also argue later (in Section 7) that it can be considered as an independent neuron model.

Theoretical analysis of some aspects of Courbage-Nekorkin-Vdovin model has been done e.g. in [44, 45]. Small networks of interacting CNV neurons have been analized in [19]. The model has been also used in biologically or clinically motivated studies, as e.g. in [64, 63, 27]. In particular, the work [43] builds discrete model of the olivo-cerebellar system basing on nonlinear version of CNV model.

Note that the earlier works ([17, 18]) discussing chaos of the map corresponding to the fast subsystem of the CNV model did not distinguish between chaos on the whole invariant interval or only on its subinterval and the analysis provided therein was not fully rigorous (though qualitatively describing the mechanism of many important properties of the full model such as chaotic spike-bursting oscillations, subthreshold oscillations and phasic spiking). The work [18] also reported numerically (see Figure 22 therein) that the invariant subset on which the dynamics of the 1D nlCNV accumulates might be the whole invariant interval or the union of subintervals. This observation is rigorously justified by us in Theorem 4.5 about the support of the acip. Further,

MOST WIEDZY Downloaded from mostwiedzy.pl

none of the earlier works studied combinatorial structure of periodic orbits which we carried out with the use of fupo theory and matched these with the spiking patterns generated.

The organization of the paper is as follows. Section 1 describes fundamentals of rotation theory applied to Lorenz-like maps. Definitions of Lorenz-like and expanding Lorenz maps and their main properties, also related to chaos, are recalled in Appendix A. Providing extensive introduction to the theory of Lorenz maps is motivated by the fact that the map $g_\alpha(x) := x + F(x) - \alpha - \beta H(x-d)$, describing the dynamics of the voltage variable x, while the second variable $y = \alpha$ is kept constant, is Lorenz-like map for large range of parameter values of interest. That fact will be crucial for our further analysis of the nlCNV model. In addition to present the state-of-the art of this theory, in section 1 and in Appendix A we prove a couple of contributing results in the general theory of Lorenz-like maps useful for investigating the dynamics of the model. In section 2 we briefly recall our results from [6] on the 1D plCNV model. Next, in section 3 we state preliminary results for the 1D nlCNV model and indicate regions in parameter space corresponding to the existence of invariant intervals on which model maps are expanding Lorenz. This allows us to apply the theory of (expanding) Lorenz maps to provide sufficient conditions for chaos in the model (Section 4) and to obtain results on rotation interval (Section 5) and itineraries of periodic orbits (Section 6). These results describe quantitatively the complexity of periodic behaviour and spike-patterns in the 1D nlCNV model. Moreover, Section 6 contains also examples and numerical simulations in which rotation intervals and itineraries of periodic orbits are computed for some choices of parameters. The theory of *fupos* and Farey-Lorenz permutations, which we widely use in Section 6, is summarized in Appendix F. In section 7 we discuss the implications of our results in terms of activity patterns and the shape of the action potential under the constant stimulus. Moreover we also go beyond the autonomous case studied in this work and include numerical examples of voltage time series generated for popular varying inputs. We also sum up the results obtained for the 1D nlCNV model and debate on their connections with the full model (4a)-(4b). Longer and technical proofs of some of our theorems are included in Appendices C, D and E.

1. Rotation theory for Lorenz maps

We will now look at the rotation theory properties related to Lorenz maps. To this end, we mainly recall definitions and results from [23], essential for our analysis of the CNV model. Let $f : [0,1] \to [0,1]$ be a Lorenz-like map (see Appendix A for definition and basic properties of Lorenz-like maps).

Definition 1.1. For a point $x \in [0,1]$ and a positive integer n we will denote by $R(x,n)$ the number of integers $i \in \{0,\dots,n-1\}$ such that $f^i(x) \in I_R$. If the limit

$$\rho(x) = \lim_{n\to\infty} \frac{R(x,n)}{n}$$

exists, we call it the *rotation number* of x.

Obviously, if x is a periodic point of f of period q, then $\rho(x)$ exists and equals $R(x,q)/q$. We have the following result ([55]) on the uniqueness of the rotation number in the nonoverlapping setting.

Theorem 1.2 (Rhodes-Thompson)**.** *If $f(0) \geq f(1)$, then all points have the same rotation number.*

In this case we denote the rotation number simply by $\rho(f)$. Therefore, in particular, nonoverlapping Lorenz-like maps admit unique rotation number. In the special case, when $f(0) = f(1)$ and f is strictly increasing on I_L and on I_R, the map can be identified with the orientation preserving homeomorphism of the unit circle $\mathbb{S}^1 = \mathbb{R}/\mathbb{Z}$. In such a situation the existence and uniqueness of the rotation number and the fact that it rational if and only if f has a periodic point follows from the classical Poincaré rotation theory (see e.g. [37]).

The alternative case $f(0) < f(1)$ can be accessed by the use of so-called water maps.

MOST WIEDZY Downloaded from mostwiedzy.pl

Definition 1.3. Let f be a Lorenz-like map and $t \in f(I_L) \cap f(I_R)$. The *water map* of f at level t is defined by

$$f_t(x) = \begin{cases} \max(t, f(x)) & \text{if } x \in I_L, \\ \min(t, f(x)) & \text{if } x \in I_R. \end{cases}$$

Note that a water map is also Lorenz-like and that $f_t(0) = f_t(1)$. Thus all points $x \in [0,1]$ have the same rotation number $\rho(f_t)$ for it. It is known (see e.g. [2] or [26, Subsec. 3.3]) that $\rho(f_t)$ is a continuous nondecreasing function of t, and, in consequence, if $f(0) < f(1)$, then $\rho(f_{f(0)}) \le \rho(f_{f(1)})$. Unfortunately, we cannot expect that in case $f(0) < f(1)$ all points in I have a well-defined rotation number. However, the following important result concerning the set of the rotation numbers of all points for which the rotation number exists holds (see [23, Sec. 2]).

Theorem 1.4. *Assume that f is a Lorenz-like map such that $f(0) > f(1)$. Then the set of the rotation numbers for f of all points having rotation number is equal to the interval* $\mathrm{Rot}(f) := \left[\rho(f_{f(0)}), \rho(f_{f(1)})\right]$. *In particular, for each $r \in \mathrm{Rot}(f)$, regardless of whether r is rational or irrational, there exists $x \in I$ such that $\rho(x) = r$.*

The set $\mathrm{Rot}(f)$ will be called the *rotation interval* of f. Finally, due to the lack of the suitable reference, we present below a sufficient condition for the existence of period 2 periodic orbit of a Lorenz-like map, which also implies that the rotation interval $\mathrm{Rot}(f)$ contains $1/2$. The proof of this result with the remark is postponed to Appendix B.

Theorem 1.5. *Let $f\colon [0,1] \to [0,1]$ be Lorenz-like map with the discontinuity point $c \in (0,1)$. Suppose that*

$$f(0) < c < f(1) \tag{7}$$

Then f has a period 2 periodic orbit. Moreover, if f is expanding, then this orbit is unstable (repelling) and is unique period 2 periodic orbit of f.

2. Two versions of one dimensional Courbage-Nekorkin-Vdovin model

Assuming the variable $y = \alpha$ is constant, the CNV model can be reduced to a one dimensional map $g\colon \mathbb{R} \to \mathbb{R}$ given by

$$g(x) = x + F(x) - \alpha - \beta H(x - d). \tag{8}$$

In general, in the above function we will vary the parameters β and/or α keeping all other parameters fixed. We consider two main versions of the 1D CNV model:

- a *piece-wise linear* case (plCNV for short), when $F(x)$ is a piece-wise linear continuous function defined as follows:

$$F(x) = \begin{cases} -m_0 x, & \text{if } x \le J_{\min}, \\ m_1(x - a), & \text{if } J_{\min} \le x \le J_{\max}, \\ -m_0(x-1), & \text{if } x \ge J_{\max}, \end{cases}$$

  where

$$m_0, m_1 > 0, \quad 1 > a > 0, \quad J_{\min} = \frac{a m_1}{m_0 + m_1}, \quad J_{\max} = \frac{m_0 + a m_1}{m_0 + m_1},$$

- a *nonlinear* case (nlCNV for short), when $F(x) = \mu x(x-a)(1-x)$ with $0 < a < 1$ and $\mu > 0$.

Observe that in both cases the function g is discontinuous at d and the plot of F has the shape of the upside down reversed $\boldsymbol{N}$ letter. However, the nonlinear map is formally simpler (has less parameters) and at the same time exhibits similarly complex dynamics. Before we study in detail the nonlinear CNV model, we briefly recall our previous results on the plCNV model from [6].

MOST WIEDZY Downloaded from mostwiedzy.pl

2.1. **1D plCNV model.** We studied piece-wise linear case (1D plCNV) in detail in our recent work [6]. In particular, we analyzed existence, location and stability of fixed points giving explicit conditions with respect to all model parameters. After restricting the model to the invariant interval (the dynamics beyond thus interval is trivial) we established the conditions for Devaney chaos and described metric properties of this model (i.e. existence and form of the absolutely continuous invariant probability measure). Moreover, the itineraries of periodic orbits were linked with patterns of spike trains fired by the 1D plCNV. Some of these results were possible due to the fact that the map defining the 1D plCNV model is a β-transformation, not general Lorenz-like map. Here, our goal is to check if and how these results transfer to the nlCNV model and identify differences between the piecewise linear and nonlinear case.

2.2. **1D nlCNV model.** In [18] the nonlinear part of the CNV model is determined by the cubic polynomial $F(x) = x(x-a)(1-x)$, which plot has the shape of the upside down reversed $\boldsymbol{N}$ letter and which has three zeroes $0 < a < 1$. Unfortunately, this assumptions seems to be too much restrictive. It occurs that in the piecewise linear case the parameter m_1 related to the derivative (slope) of the function F plays crucial role in creating interesting dynamics. To obtain similar control on the slope of F we have decided to introduce a new parameter $\mu > 0$ and define $F(x)$ as $\mu x(x-a)(1-x)$. It is worth pointing out that such a parameter appears often in some versions of the FitzHugh-Nagumo model, which was one of the main motivations for the 2D CNV model. So finally, in our paper the nlCNV function $g\colon \mathbb{R} \to \mathbb{R}$ is defined as

$$g(x) = x + \mu x(x-a)(1-x) - H^d_{\alpha,\beta}(x), \tag{9}$$

where

$$H^d_{\alpha,\beta}(x) = \begin{cases} \alpha, & \text{if } x < d, \\ \alpha + \beta, & \text{if } x \geq d. \end{cases}$$

Following [18] we will also assume that $\beta > 0$ and the discontinuity point d lies between the extrema of the function F. Detailed results on the 1D nlCNV model are presented in the rest of the paper.

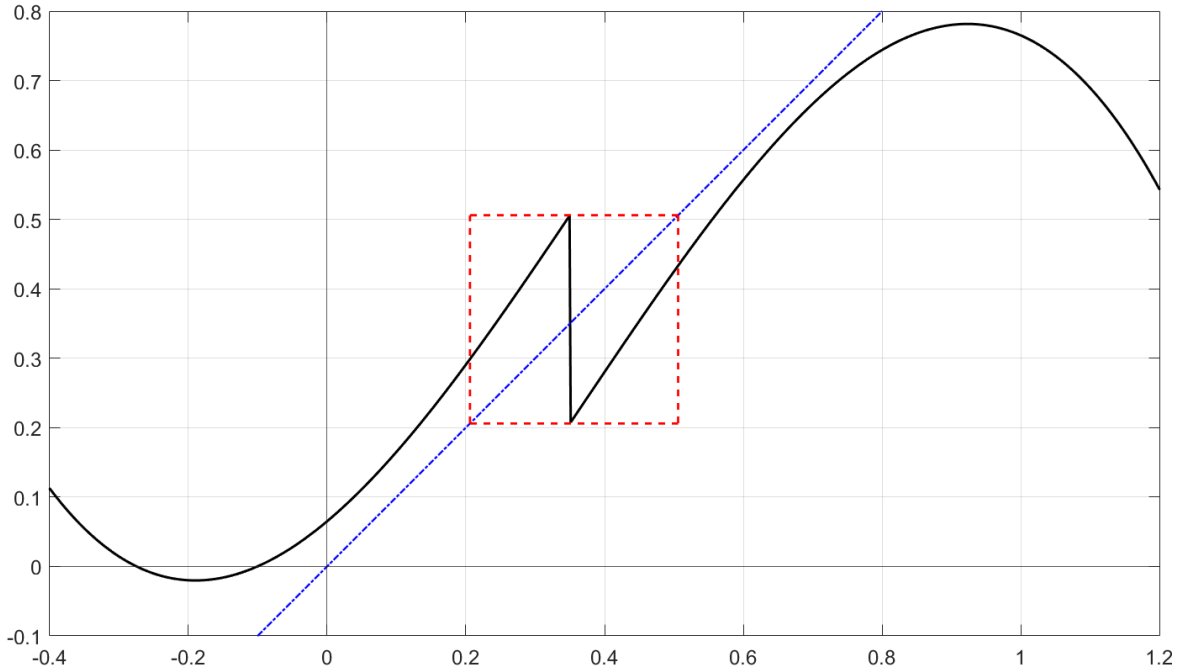

FIGURE 1. Plot of the nlCNV function (in black) and the invariant interval (denoted by a square of dashed lines). Parameter values: $\mu = 1.6$, $a = 0.1$, $d = 0.35$, $\alpha = -0.065$, $\beta = 0.3$.

MOST WIEDZY Downloaded from mostwiedzy.pl

3. Analysis of invariant intervals for 1D nlCNV model

This section is devoted to the study of the basic dynamical properties of the 1D nlCNV model, i.e., the function

$$g(x) = x + \mu x(x-a)(1-x) - H^d_{\alpha,\beta}(x) = x + F(x) - H^d_{\alpha,\beta}(x) = f(x) - H^d_{\alpha,\beta}(x).$$

Namely, we will examine the existence of the invariant interval, on which the 1D nlCNV function is an expanding Lorenz map (see Figure 1). The ends of this interval are given, similarly as in the piecewise linear case, by the formulas

$$b = \lim_{x\to d^+} g(x) = g(d) = d + F(d) - \alpha - \beta,$$
$$c = \lim_{x\to d^-} g(x) = d + F(d) - \alpha.$$

Let $x_{\min}$ and $x_{\max}$ denote the points of local minimum and maximum of the cubic polynomial F. An immediate calculation gives

$$x_{\min} = \frac{a+1-\sqrt{a^2-a+1}}{3} \quad \text{and} \quad x_{\max} = \frac{a+1+\sqrt{a^2-a+1}}{3}.$$

We will work here with the three general assumptions

- $0 < a < 1$,
- $\mu > 0$,
- $x_{\min} < d < x_{\max}$,

which are quite natural and does not seem to be very restrictive. Now let us assume that values of a, μ and d are fixed and satisfy the above conditions. We will search for the values of α and β for which the restriction of g to the interval $[b, c]$ is an expanding Lorenz map. It is easy to observe that to guarantee this we need the following additional assumptions:

- $x_{\min} < b < d < c < x_{\max}$,
- $g(b) \geq b$ and $g(c) \leq c$.

Table 1 shows how the above conditions can be translated in the terms of parameters α and β. Since $[b, c] \subset (x_{\min}, x_{\max})$, we obtain immediately that $F'(x) > 0$ and, in consequence, $g'(x) > 1$

Table 1. Conditions for the existence of an invariant interval.

No.	Condition	Parametric form
1.	$x_{\min} < b$	$\beta < d + F(d) - x_{\min} - \alpha$
2.	$c < x_{\max}$	$\alpha > d + F(d) - x_{\max}$
3.	$b < d$	$\beta > F(d) - \alpha$
4.	$d < c$	$\alpha < F(d)$
5.	$g(b) \geq b$	$\alpha \leq F(d + F(d) - \alpha - \beta)$
6.	$g(c) \leq c$	$\beta \geq F(d + F(d) - \alpha) - \alpha$

for $x \in [b, c]$, which is required in the definition of an expanding Lorenz map.

Let G denote g restricted to $[b, c]$. Let us summarize the first result concerning the 1D nlCNV model.

Theorem 3.1 (expanding Lorenz map)**.** *Assume that the conditions 1–6 listed in Table 1 are satisfied. Then the map $G\colon [b, c] \to [b, c]$ is a well-defined expanding Lorenz map.*

Now let us look for the answer to the following question. Assuming a, μ and d are fixed can we always find the values of α and β for which the conditions 1–6 hold? Fortunately, the answer is positive under quite mild assumptions as we can see below. The technical proof of Theorem 3.2 is postponed to Appendix C.

Theorem 3.2 (existence of invariant interval)**.** *If $F'(d) < 1$ then the subset of the plane α-β for which the conditions 1–6 are true is nonempty (in fact it has positive Lebesgue measure).*

MOST WIEDZY Downloaded from mostwiedzy.pl

It remains to check when the condition $F'(d) < 1$ holds. As expected we obtain some mild restriction on the parameter μ responsible for the slope of F.

Proposition 3.3 (conditions for invariant interval)**.** *For any arbitrary values of parameters* $a \in (0,1)$, $d \in (x_{\min}, x_{\max})$ *and* $\mu \in (0,3]$ *we have* $F'(d) < 1$.

Proof. Since

$$F'(x) = \mu(-3x^2 + 2(a+1)x - a),$$

it is enough to show that for each $x \in (x_{\min}, x_{\max})$

$$w(x) = -3x^2 + 2(a+1)x - a < 1/\mu,$$

if $0 < a < 1$ and $0 < \mu \leq 3$. Note that $w(x)$ attains maximum at the point $x = (a+1)/3$ and the maximum value is $\frac{1}{3}(a^2 - a + 1)$. But $a^2 - a + 1 < 1$ for $a \in (0,1)$ and, in consequence, $w(x) < 1/3 \leq 1/\mu$, which is the desired conclusion. □

The left panel of Figure 2 provides an illustration of how the set of parameters from Theorem 3.2 may look like if the conditions 1–6 are satisfied. In fact, for the chosen parameter values (see the caption of Figure 2) we have $F'(d) \approx 0.607 < 1$. Black lines on the left panel correspond to the borders of areas described by the conditions 1–6. The red area shows parameter values of α and β for which G is an expanding Lorenz map. Geometrically, this area is a subset of the parallelogram (conditions 1–4) between the two nonlinear curves (conditions 5–6). In turn, the right panel shows how the conditions for α and β can be translated into the conditions for b and c (endpoints of the invariant interval). We simply use the linear change of coordinates given by the formulas for b and c. In other words, the right panel presents the set of pairs (b,c) corresponding to invariant intervals for expanding Lorenz maps. Note that the red area is contained in the square $[x_{\min}, x_{\max}]^2$ between the plot of the function $x \mapsto f(d) - F(x)$ and its inverse function. Symmetry of the red area in the right panel is related to the choice of d as $(x_{\min} + x_{\max})/2$.

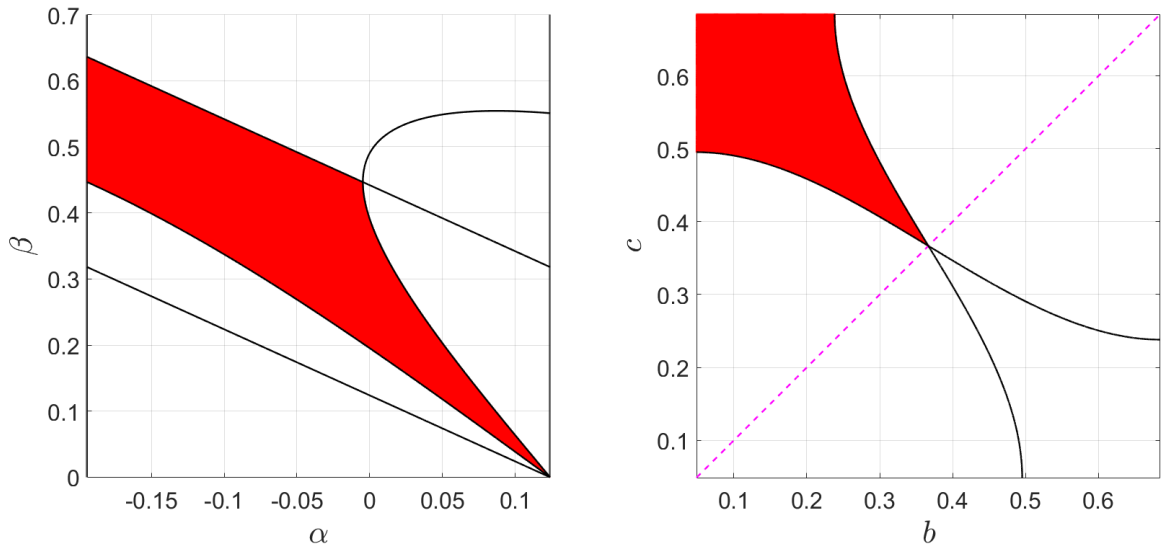

FIGURE 2. Set of parameters α-β for which the conditions 1–6 hold and, in consequence, the invariant interval exists (left in red) and the respective set of possible endpoints (b the beginning and c the end) of invariant intervals (right in red) for parameter values: $\mu = 2$, $a = 0.1$, $d = 0.367$ (case $F'(d) < 1$ covered by Theorem 3.2).

Remark 3.4. Even if $F'(d) \geq 1$, the set of α and β for which the conditions 1–6 hold may be nonempty as shows Figure 3 (here $\mu = 4$ and $F'(d) \approx 1.21$). Observe that compared to Figure 2 the red area on Figure 3 occupies a relatively much smaller part of the parallelogram given by

MOST WIEDZY Downloaded from mostwiedzy.pl

the conditions 1–4. Moreover, in that case it is rather hard to formulate the nice condition for the existence of the invariant interval similar to that formulated in Theorem 3.2. However, if the parameter μ will be big enough, then the set of parameters α and β for which the conditions 1–6 are satisfied may be empty (this is the case when $\mu = 5$, $a = 0.1$, $d = 0.367$).

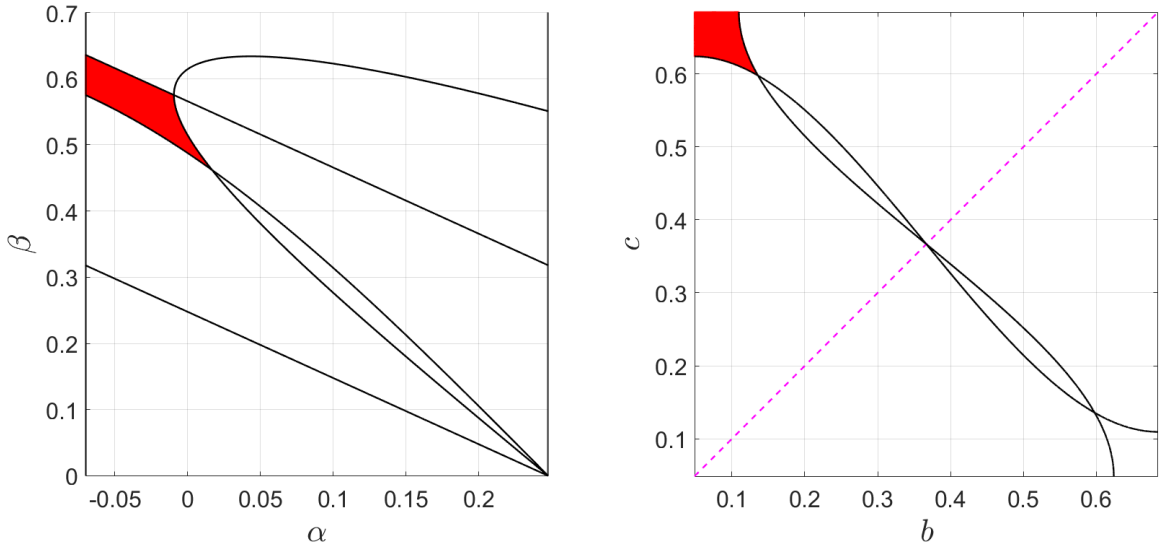

FIGURE 3. Set of parameters α-β satisfying the conditions 1–6, i.e., guaranteeing the existence of the invariant interval (left in red) and the respective set of possible endpoints (b,c) of invariant intervals (right in red) for parameters values: $\mu = 4$, $a = 0.1$, $d = 0.367$ (case $F'(d) \geq 1$, which is not covered by Theorem 3.2).

4. Chaotic behaviour in the 1D nlCNV model

This section, divided into three subsections, is devoted to examine main chaotic properties of the 1D nlCNV model.

4.1. Conditions for chaos for a single model map.

Below we present a sufficient condition for chaotic dynamics in terms of the derivative of the model map. Let $\lambda = \inf\{G'(x) \mid x \in [b,c]\}$.

Theorem 4.1. *If one of the following conditions is satisfied:*

(i) $\sqrt{2} \leq \lambda \leq 2$,
(ii) $\sqrt[3]{2} \leq \lambda < \sqrt{2}$ *and* $G(b) - b \geq \frac{\beta}{1+\lambda}$,
(iii) $\sqrt[3]{2} \leq \lambda < \sqrt{2}$ *and* $c - G(c) \geq \frac{\beta}{1+\lambda}$,

then G is chaotic in the sense of Devaney on the interval $[b,c]$. It is also strongly transitive and mixing.

Proof. It is a consequence of Theorem A.8 after scaling the interval $[0,1]$ to $[b,c]$, i.e., by the factor β. □

Finally, note that as an expanding Lorenz map G is also expansive without any assumptions (see Appendix A). Conditions of Theorem 4.1 might be hard to verify analytically. However, Lemma 4.2 yields a bit more explicit expression for λ.

Lemma 4.2. *To determine whether the 1D nlCNV model is chaotic, it suffices to estimate the value of G' at the endpoints of the invariant interval $[b,c]$:*

(1) Suppose that $b \geq \frac{1+a}{3}$. Then $\lambda = G'(c)$.
(2) Suppose that $c \leq \frac{1+a}{3}$. Then $\lambda = G'(b)$.
(3) If $b < \frac{1+a}{3} < c$, then $\lambda = \min\{G'(b), G'(c)\}$.

In particular, it always holds that $\lambda = \min\{G'(b), G'(c)\}$.

MOST WIEDZY Downloaded from mostwiedzy.pl

Proof. Differentiating G twice yields $G''(x) = 2\mu(1 + a - 3x)$ from which it follows that $G'(x)$ is increasing for $x < \frac{1+a}{3}$ and decreasing for $x > \frac{1+a}{3}$. □

4.2. **Conditions for the existence of chaos in the α-β parameter plane.** In this subsection we provide sufficient conditions for nonemptiness of the set of parameters that guarantee Devaney's chaos on the whole invariant interval. Let us begin with a brief analysis of the quadratic equation $G'(x) = \sqrt{2}$, i.e.,

$$-3\mu x^2 + 2\mu(a+1)x + 1 - \mu a = \sqrt{2}.$$

Note that this equation has two distinct real roots (denote them by $x_1 < x_2$) if and only if $\Delta = 4\mu(\mu a^2 - \mu a + \mu - 3\sqrt{2} + 3) > 0$ or, equivalently, $\mu > 3(\sqrt{2}-1)/(a^2 - a + 1)$. An immediate computation shows that

$$x_{1,2} = \frac{\mu(a+1) \mp \sqrt{\mu\left(\mu a^2 - \mu a + \mu - 3\sqrt{2} + 3\right)}}{3\mu}$$

Now, let A denote the set of parameters α-β for which G is an expanding Lorenz map on the invariant interval $[b, c]$. Let us formulate the sufficient condition the existence of chaos parameters in the α-β plane.

Theorem 4.3. *Assume that $a \in (0,1)$, $d \in (x_{\min}, x_{\max})$ and $\mu \in (0,3]$, which implies that A is nonempty (has positive Lebesgue measure). If, in addition,*

$$\mu > \frac{3\left(\sqrt{2}-1\right)}{a^2 - a + 1} \quad \text{and} \quad x_1 < d < x_2, \tag{10}$$

then the subset $C \subset A$ consisting of parameters α-β, for which G is chaotic on the interval $[b, c]$, is also nonempty (contains a set of positive Lebesgue measure).

The proof of Theorem 4.3 is postponed to Appendix D.

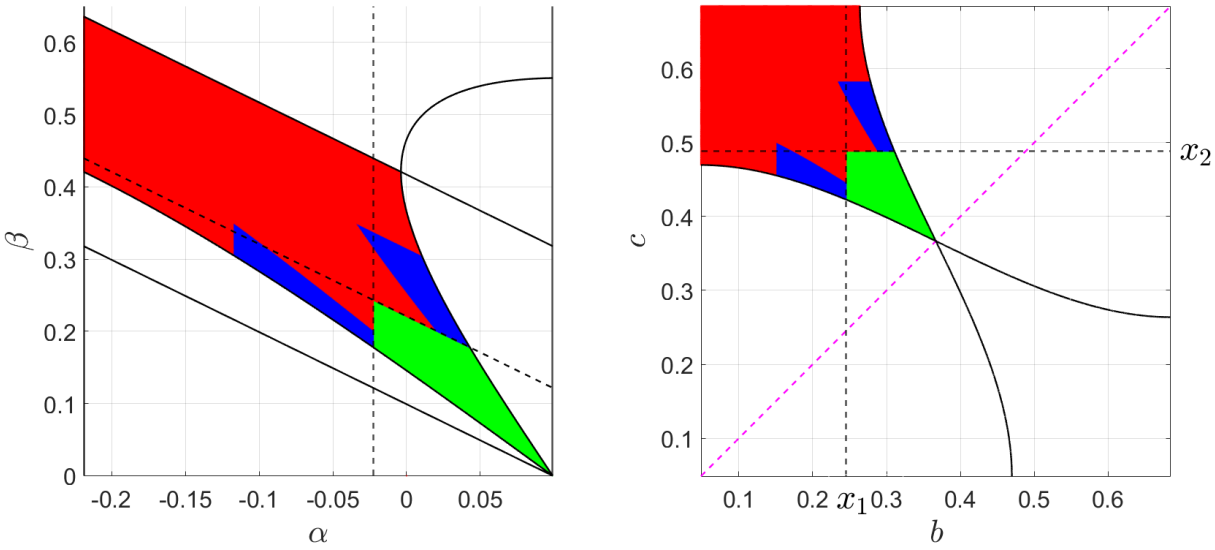

FIGURE 4. Set of parameters α-β for which the conditions (from Thm 4.1) sufficient for chaos existence hold. On the left panel in green area corresponding to Thm 4.1 (i) and in blue area corresponding to Thm 4.1 (ii) and (iii). On the right panel the respective sets of possible endpoints of "chaotic" invariant intervals (in green and blue). Other parameter values: $\mu = 1.6$, $a = 0.1$, $d = 0.367$.

It may be interesting to compare both size and location of areas in the α-β parameter plane related to different chaos conditions from Theorem 4.1. Figure 4 presents the result of our numerical simulations: in green we see the area corresponding to the simpler condition $\sqrt{2} \le \lambda \le 2$ and in

MOST WIEDZY Downloaded from mostwiedzy.pl

blue the area corresponding to the more complex condition $\sqrt[3]{2} \leq \lambda < \sqrt{2}$ and $(G(b) - b \geq \frac{\beta}{1+\lambda}$ or $c - G(c) \geq \frac{\beta}{1+\lambda})$.

Remark 4.4. Note that the "chaos existence condition" (10) from Theorem 4.3 can be formulated for all $a \in (0,1)$ simultaneously (full parameter range). Since $a^2 - a + 1 \geq 3/4$, we obtain the estimation

$$\mu > 4\left(\sqrt{2} - 1\right) \approx 1.6569$$

Alternatively, it can be calculated for the fixed value of a, which gives in general sharper estimations. For example, if $a = 0.1$, we obtain the condition

$$\mu > \frac{3\left(\sqrt{2} - 1\right)}{0.91} \approx 1.3655$$

In fact, the inequality (10) provides nice functional dependence between μ and a. Namely, let $\mu_0(a) = 3\left(\sqrt{2} - 1\right)/(a^2 - a + 1)$, i.e., $\mu_0(a)$ is the threshold above which the values of μ (up to 3) guarantee for a given a, according to Theorem 4.3, the existence of nonempty chaos area. Then the μ_0 as a function of a is symmetric unimodal with maximum at $a = 0.5$.

4.3. **Ergodicity and acip.** The hierarchy of chaos often starts from *ergodicity*, which alone is of course barely considered as real chaos. For that reason it is worth emphasizing that the nlCNV map restricted to the invariant interval is always *ergodic*, which is a natural prerequisite for chaos.

Recall first a few notions of ergodic theory. Let $f\colon [b,c] \to [b,c]$ be an expanding Lorenz map and λ be a measure on the interval $[b,c]$. We say that

- f *preserves measure* λ or that λ is f*-invariant* if $\lambda\left(f^{-1}(B)\right) = \lambda(B)$ for all measurable sets B,
- a measure-preserving f is *ergodic* if for any measurable B, such that $f^{-1}(B) = B$, $\lambda(B) = 0$ or $\lambda([b,c] \setminus B) = 0$.

Since ergodicity is a property of the pair (f, λ), we often say that f has an ergodic measure λ.

We use the standard abbreviation *acip* for an f-invariant probability measure that is absolutely continuous with respect to the Lebesgue measure of $[b,c]$. Given a measure λ, the *support* of λ (denoted by $\mathrm{supp}(\lambda)$) is the smallest closed set of full λ-measure. Note that the following result does not require any extra assumptions apart from the existence of invariant interval.

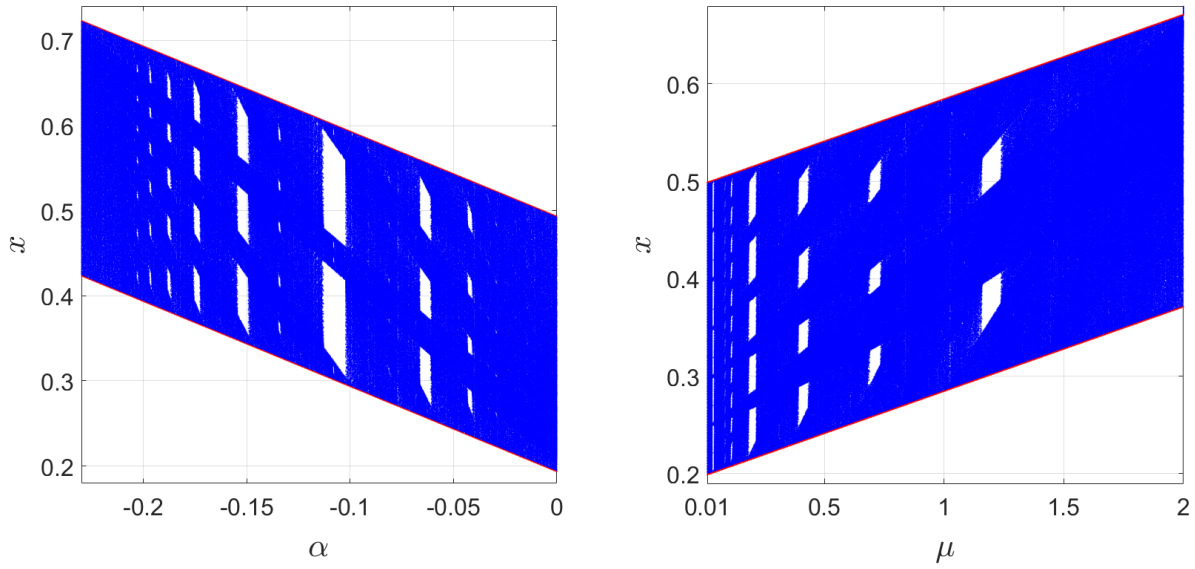

FIGURE 5. Bifurcation diagrams for the family of nlCNV maps with respect to α (left) and μ (right). Other parameter values: $a = 0.1$, $d = 0.45$, $\beta = 0.3$, $\mu = 0.5$ (left) and $\alpha = -0.048$ (right).

MOST WIEDZY Downloaded from mostwiedzy.pl

Theorem 4.5. *Under the conditions 1–6 from Table 1 the map $G\colon [b,c] \to [b,c]$ has a unique ergodic acip measure and the support of this measure is a finite union of closed intervals.*

Proof. Recall that any piecewise C^1-function f is of bounded variation and if, in addition, f is separated from 0, i.e., $|f| \geq \sigma > 0$ for some $\sigma > 0$, then the reciprocal $1/f$ is also of bounded variation. Since the map G is piecewise C^2 and $|G'| \geq \sigma > 1$, it satisfies the assumptions of Theorems 5.2.1, 8.2.1 and 8.2.2 in [8]. Now our assertion follows immediately from these three results. □

Remark 4.6. Observe that any ergodic measure-preserving map on the interval (more generally, on compact metric space) is topologically transitive on $\operatorname{supp}(\lambda)$ (see for instance Exercise 6.15 in [11]). Hence, if $\operatorname{supp}(\lambda)$ is the whole domain $[b,c]$, then the map is transitive on $[b,c]$ and, in consequence, is chaotic in the sense of Devaney on $[b,c]$ from Theorem A.8.

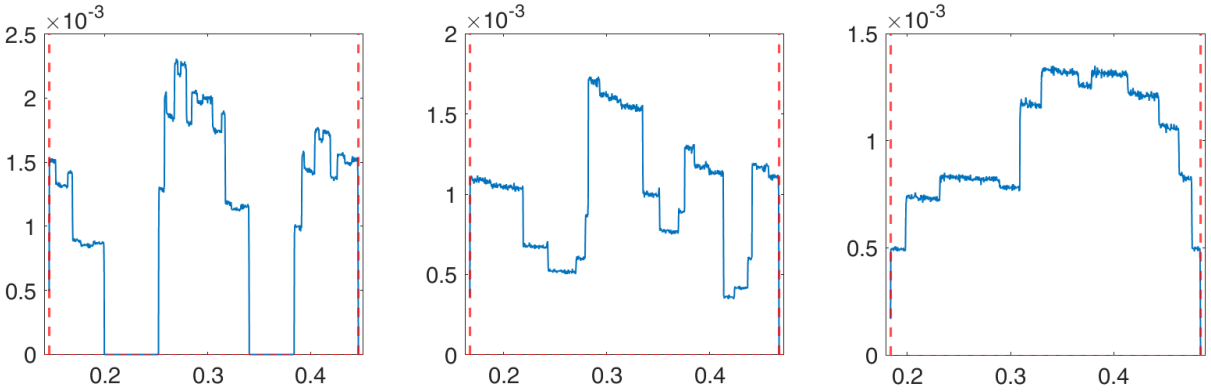

FIGURE 6. Distributions of probability density functions, i.e., frequencies of visits to different parts of the invariant interval for three values of the parameter μ: $\mu = 1.1$ (left), $\mu = 1.6$ (middle), $\mu = 2$ (right). Other common parameter values: $a = 0.1$, $d = 0.3$, $\alpha = -0.1$, $\beta = 0.3$.

Numerically, the fact that the support of the acip measure consists of a finite union of closed intervals can be clearly observed on the bifurcations diagrams for the nlCNV family of maps (see Figure 5). Namely, notice the appearance and the location of "white gaps" in the bifurcation diagram, which corresponds to the situation when the support of acip is not the whole interval $[b,c]$ but the union of a finite number of smaller disjoint intervals. Observe that "white gaps" only appear for relatively small values of μ and, in consequence, values of $\lambda = \inf\{G'(x) \mid x \in [b,c]\}$ just above 1.

Moreover, the numerical analysis (see Figure 6) shows that the probability density function of acip in our model is far from being uniform. However, the analysis also suggests that the probability distribution is more regular (flattened) for higher values of $\lambda = \inf\{G'(x) \mid x \in [b,c]\}$. In Figure 6 these values are respectively: $\lambda = 1.17$ (left), $\lambda = 1.29$ (middle), $\lambda = 1.41$ (right).

5. Periodicity and rotation interval for the 1D nlCNV model

In this section we discuss topics related to periodicity and rotation interval for the model map. Here, unless stated otherwise, we assume that the conditions 1–6 are satisfied, i.e. the map defining the voltage dynamics in the 1D nlCNV model is an expanding Lorenz map.

5.1. Fixed points of the 1D nlCNV map.

The following observation can be easily justified by the fact that the map $G : [b,c] \to [b,c]$ is expanding:

- the only possible fixed points of G are b and c; in particular, if $G(b) = b$ (or $G(c) = c$), then the rotation interval of G $\operatorname{Rot}(G)$ contains 0 (respectively, 1),
- if $G(b) > b$ and $G(c) > c$, then G does not have fixed points.

MOST WIEDZY Downloaded from mostwiedzy.pl

5.2. **Period-2-periodicity condition for a single model map.** Below we provide a geometric condition for the existence of period two periodic orbit in this system, which is an immediate consequence of Theorem 1.5.

Lemma 5.1. *Let $G : [b, c] \to [b, c]$ be the expanding Lorenz map describing the 1D nlCNV model. Suppose that*

$$G(b) < d < G(c). \tag{11}$$

Then G has exactly one period-2 periodic orbit and consequently $\frac{1}{2} \in \mathrm{Rot}(G)$. This orbit is repelling.

5.3. **Conditions for the existence of a 2-periodic orbit in the α-β parameter plane.** Let A denote the set of parameters α-β for which G is an expanding Lorenz map. Note that the following result does not require any new additional assumptions (compare Theorem 3.2). Its proof is postponed to Appendix E.

TABLE 2. Conditions for the existence of a 2-periodic orbit.

No.	Condition	Parametric form
10.	$g(b) < d$	$F(d + F(d) - \alpha - \beta) + F(d) - 2\alpha - \beta < 0$
11.	$g(c) > d$	$F(d + F(d) - \alpha) + F(d) - 2\alpha - \beta > 0$

Theorem 5.2. *Assume that $F'(d) < 1$, which implies that A is nonempty (has positive Lebesgue measure). Then the subset $B \subset A$ consisting of parameters α-β for which G has a 2-periodic orbit is also nonempty (has positive Lebesgue measure).*

Remark 5.3. Numerical simulations in MATLAB show that for some choice of the parameter μ the set B is a proper subset of A and for the other choice $B = A$. Figure 7 presents both cases. On the left panel the yellow area of parameters corresponding to the existence of a 2-periodic orbit lies strictly inside the red area corresponding to invariant interval parameters ($\mu = 1.6$, $a = 0.1$, $d = 0.367$). In the right panel the yellow area covers the whole red area ($\mu = 3$, $a = 0.1$, $d = 0.367$), which means that if we have an invariant interval, we also have a 2-periodic orbit.

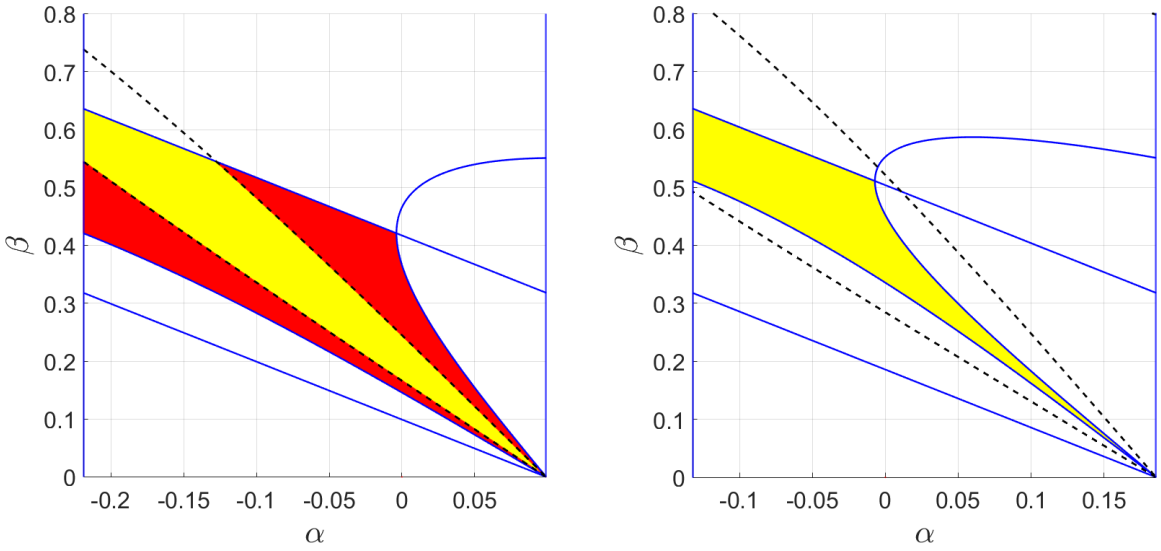

FIGURE 7. Regions of parameters giving a 2-periodic orbit (in yellow) inside the areas corresponding to invariant interval (in red). On the right panel yellow region fully covers the red area. Main parameter: $\mu = 1.6$ (left) and $\mu = 3$ (right). Other common parameter values: $a = 0.1$, $d = 367$.

MOST WIEDZY Downloaded from mostwiedzy.pl

5.4. **Analysis of rotation interval.** *Rotation numbers* were defined by H. Poincaré for circle homeomorphisms and diffeomorphisms to characterize the set of periods of these maps. These real numbers between 0 and 1 naturally generalize the usual geometric rotation angle (modulo 2π) for circle translations. Interestingly, they occurred to be quite useful in the number of applications, especially in complex dynamics. In 1983 Newhouse, Palis and Takens (see [48]) extended the notion of rotation number to continuous circle maps of degree one. Instead of a single number they got in general a closed interval, which they called *rotation set* or *rotation interval*. The original rotation number for homeomorphisms does not depend on the choice of the point on the circle. However, for a continuous circle map (not homeomorphism) we may obtain different rotation numbers starting from different points. Now the collection of rotation numbers computed for all points on the circle forms the rotation interval. Finally and maybe a bit surprisingly, the rotation theory works fine also for discontinuous circle maps ([26]) and Lorenz-like maps ([23]).

The notions of rotation number and rotation interval have found various applications. In particular, they appear in situations where circle maps arise naturally and are connected with phenomenon of *phase-locking*. Among others, they are used in modelling of electronic oscillators, cardiac rhythms, heart arrhythmias and other biological clocks ([3, 24]). In the context of neuroscience, the rotation theory is a tool to qualify and explain firing rates and neural oscillations, both at the level of large neuronal circuits (see e.g. [54]) as well as at the level of a single cell (see e.g. [9, 22, 36, 51]).

In our setting, roughly speaking, the meaning of the rotation interval is as follows. If a number p/q (p, q coprime) is in the rotation interval of a Lorenz-like map defined on $[0, 1]$, then this map has a periodic orbit of period q such that exactly p points of the periodic orbit are contained in the right subinterval $[c, 1]$ of the domain, where c is a discontinuity point. The precise formulation of this observation is given by Proposition F.8.

As we see, the rotation interval provides important information on the periodic behaviour of a map. In a nutshell, the larger rotation interval the bigger periodic diversity. Since to all rational fractions p/q (p, q coprime) correspond some q-periodic orbits, we see that in general bigger rotation intervals admit abundance of shorter periods, but, of course, do not exclude long ones. Conversely, smaller rotation intervals yield rather mainly longer periods. Actually, the mechanism of producing periodic orbits with different periods is much more complicated and will be described in detail in the next section.

It is well-known (see e.g. [26]) that

- the rotation number and, in consequence, the endpoints of the rotation interval *depend continuously* on the map in the norm of uniform convergence,
- the rotation number is *monotonic*, i.e., $f \geq g$ implies $\rho(f) \geq \rho(g)$,
- the plot of the rotation number often contains of a version of a *devil's staircase*,

but instead of providing rigorous results of that type concerning the 1D nlCNV map we present the numerical analysis of rotation interval for the model with respect to different parameters. This analysis shows that all three phenomena mentioned above occur numerically in our simulations.

In this subsection the graphs of the rotation intervals for the 1D nlCNV map are plotted as functions of three main parameters of our model: α, β and μ. Since the functional dependence in each of these three case follows different pattern, we present here three separate plots. On all figures we can observe two main effects: when one of the parameters varies the rotation interval moves up or down and it shrinks or expands. Moreover, these two processes usually occur simultaneously. Note that usually the length of the rotation interval is not monotonic as a function of a parameter. However, we can sometimes observe some general tendencies like shrinking and expanding of the interval.

Figure 8 shows the dependence of the rotation interval on α, which is the parameter corresponding to the second variable in the 2D CNV model. The distinguishing feature is its symmetry. In the center of symmetry the interval seems to degenerate to a single point. In turn on Figure 9 we see

MOST WIEDZY Downloaded from mostwiedzy.pl

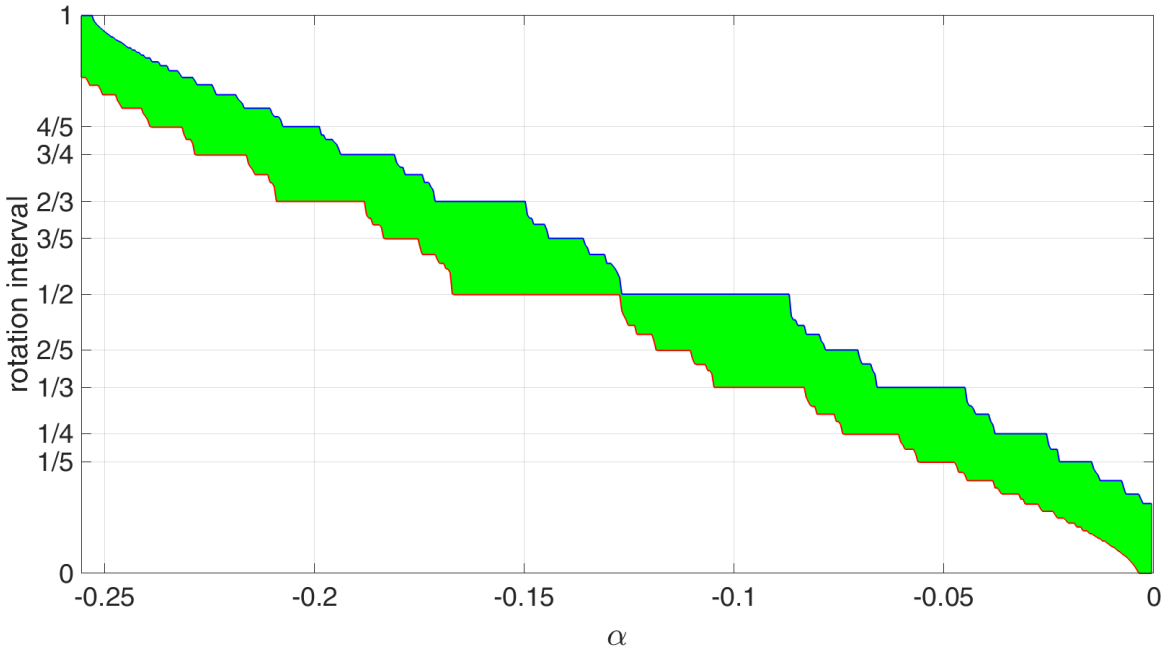

FIGURE 8. Dependence of rotation interval (in green) on the parameter α for the nlCNV map family. Other parameter values: $a = 0.1$, $d = 0.37$, $\beta = 0.455$, $\mu = 1.6$.

dependence on β (the length of invariant interval). In general as a trend, the larger β the smaller rotation interval. However, shrinking is not monotonic, but rather oscillatory.

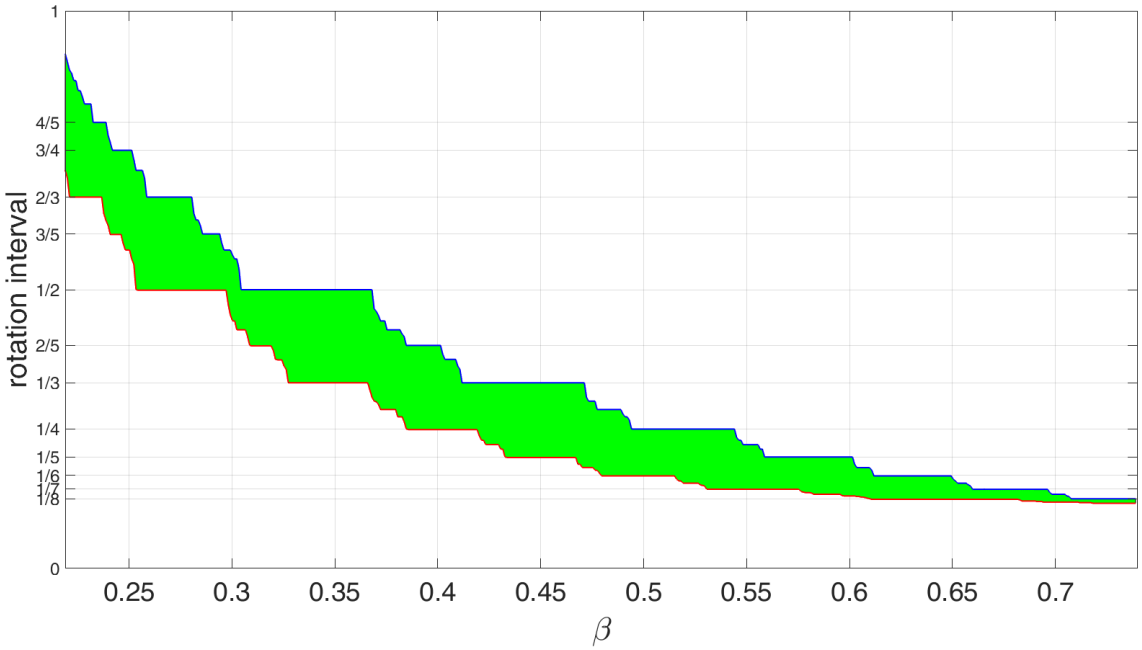

FIGURE 9. Dependence of rotation interval (in green) on the parameter β for the nlCNV map family. Other parameter values: $a = 0.1$, $d = 0.37$, $\alpha = -0.05$, $\mu = 1.6$.

Finally, Figure 10 presents dependence on μ, which controls the size of nonlinearity in our model. Here, we can observe quite rapid (but once more not entirely monotonic) expanding of the rotation interval. It is worth emphasising that the range of rotation interval plays crucial role in the considerations of the next section.

MOST WIEDZY Downloaded from mostwiedzy.pl

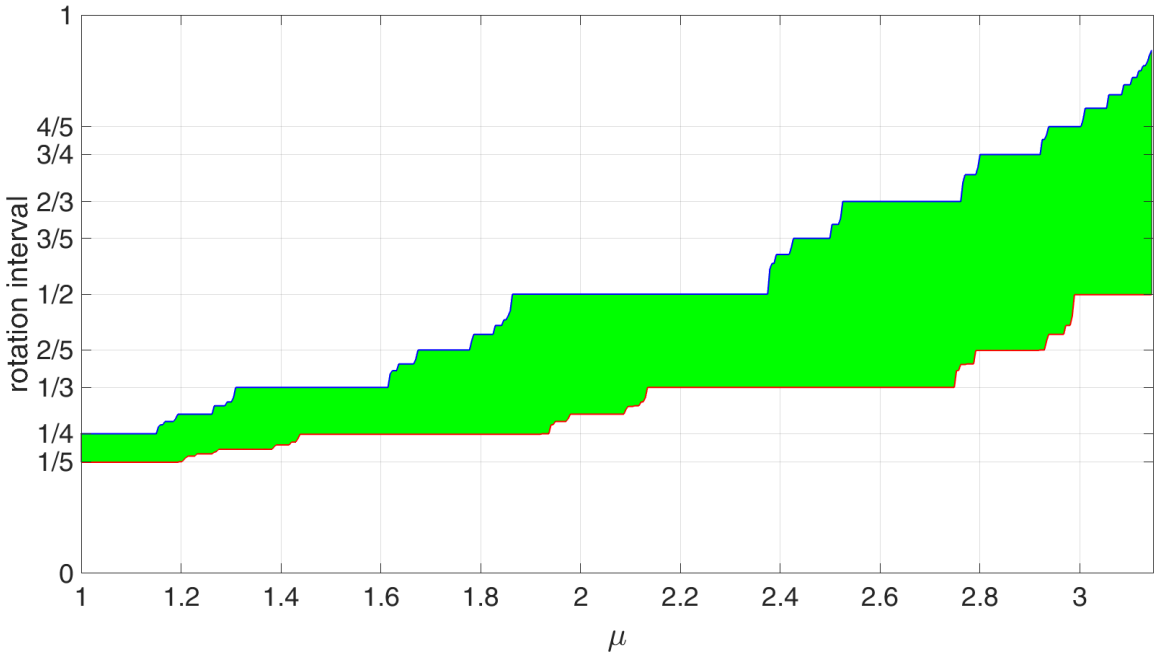

FIGURE 10. Dependence of rotation interval (in green) on the parameter μ for the nlCNV map family. Other parameter values: $a = 0.1$, $d = 0.37$, $\alpha = -0.065$, $\beta = 0.455$.

6. Orbit itineraries and complexity of spike-trains

This section consisting of two subsections develops and continues the analysis of periodic behaviour of the model. In order to address the question of the structure of periodic orbits in the CNV model, we will rely on the notions of *fupos* and FL-permutations. This allows to derive a large subset of periodic orbit itineraries which then can be linked with patterns of spike trains fired by a neuron.

Theory of periodic orbits and their finite concatenations (*fupos*) is presented in Appendix F, relying on the results from [23] (most of them are also summarized in [6]). An example of a *fupo* in the 1D nlCNV model is shown in Figure 11.

6.1. Complexity of spiking patterns.

In our previous work [6] we have identified the itineraries of periodic orbits with spike patterns fired by the 1D CNV model. In particular, basing on Corollaries 3, 4 and 5 therein we can formulate the following useful observation for the 1D nlCNV model.

Proposition 6.1. *Assume that the conditions 1-6 listed in Table 1 hold. If $p/q \in \mathrm{Rot}(G)$ (p and q coprime), where G defines the 1D nlCNV model, then there is a q-periodic voltage-train (with $q-p$ time instances at which the membrane voltage increases and p time instances of the decrease in the voltage). Moreover, there are at most $\binom{q}{p}/q$ such periodic spike trains, each of different itineraries. Among them, there exists a unique q-periodic spiking pattern with the itinerary of the form $(\tilde{x}_1, \tilde{x}_2, \ldots, \tilde{x}_q)$ (where $\tilde{x}_i \in \{L, R\}$) such that $\tilde{x}_i = L$ if and only if $1+(i-1)p \mod q \leq q-p$ (with L-symbols corresponding to the increase in the neuron's membrane potential and R with the decrease). If the occurrence of the word LR is interpreted as a spike, then this spike train features n spikes in each q-cycle, where*

$$n := \#\{1 < j < q \mid 1+(j-1)p \mod q \leq q-p \text{ and } 1+jp \mod q > q-p\}$$

(with the convention that $q \mod q = q$).

Moreover, from Theorem F.10 we immediately obtain the following fact.

Proposition 6.2. *Assume that the conditions 1-6 listed in Table 1 hold. If $[a/p, b/q] \subset \mathrm{Rot}(G)$, where $a/p < b/q$ are Farey neighbours and $p < q$, then there exist twist periodic orbits P and Q, with*

MOST WIEDZY Downloaded from mostwiedzy.pl

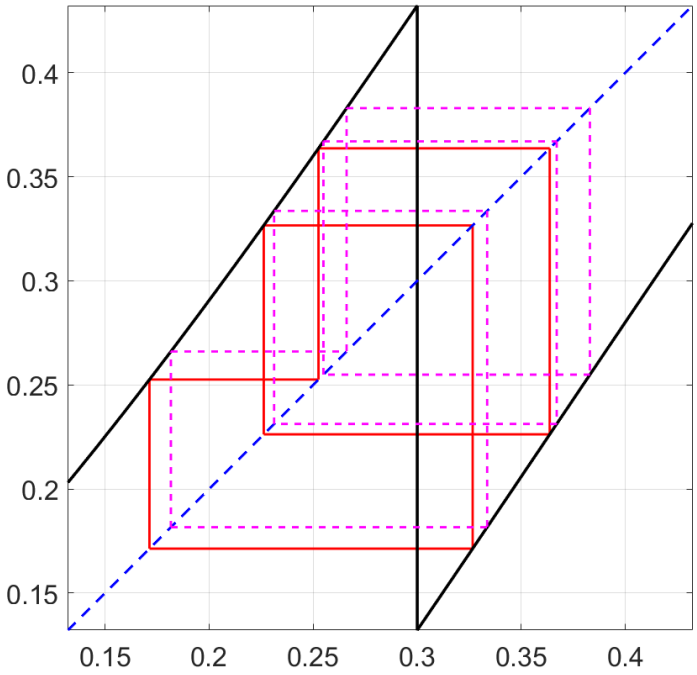

FIGURE 11. Fupo (two periodic orbits of periods 5 and 7) of FL-type corresponding to rotation numbers being Farey neighbours: $2/5 < 3/7$. This fupo appears in the nlCNV model with parameter values: $\mu = 1.6$, $a = 0.1$, $d = 0.35$, $\beta = 0.3$, $\alpha = -0.065$.

rotation numbers a/p and b/q respectively, and each itinerary, which is a concatenation of finitely many periodic itineraries of P and Q, corresponds to the exactly one periodic spike train fired by the 1D nlCNV model.

Figure 12 presents three types of periodic spiking behaviour (lower panel) of the 1D nlCNV model together with related orbits of the Lorenz map G (upper panel). In particular we see twist periodic orbits corresponding to Farey neighbours $2/3$ and $3/4$ (left and centre, respectively) and the fupo of $2/3 < 3/4$ type, obtained as a concatenation of one copy of the $2/3$-twist periodic orbit and two copies of the $3/4$-twist periodic orbit, as described by Proposition 6.1. The periodic orbit obtained in this way has rotation number equal to $8/11$ and itinerary $LRRLRRRLRRR$.

Note that Propositions 6.1 and 6.2 do not cover the whole complexity of attainable spike patterns since there might be other periodic orbits which are not necessarily a concatenation of periodic itineraries of this form as well as many nonperiodic orbits. These propositions also do not imply how a "typical" spike pattern observed looks like since the periodic orbits cannot be stable as the map g is expanding under conditions 1-6. Therefore a firing pattern highly depends on the initial condition and one can mostly expect "irregular" spiking trains, as the one depicted in Figure 13, which was obtained for the same parameter values as Figure 12 presenting periodic-like behaviour. The fact that a randomly chosen orbit looks chaotic and that it is practically impossible to find numerically purely periodic orbits is also confirmed by the results of the so-called 0-1 Chaos Test (see [25]) carried by us, which returned values very close to 1 (see Figure 14).

Observe that the periodic orbit with given itinerary is always unique (and unstable), as the map G is expanding, and therefore finding numerically such a periodic is very challenging. Thus the method of fupos, as described by Propositions 6.1 and 6.2, enables to deduce the existence of infinitely many periodic spiking patterns of the 1D CNV model, which, due to the above mentioned reasons, would be rather impossible to find numerically and often, especially in case of long periods, also analytically. On the other hand, the knowledge on the existence of such periodic patterns,

MOST WIEDZY Downloaded from mostwiedzy.pl

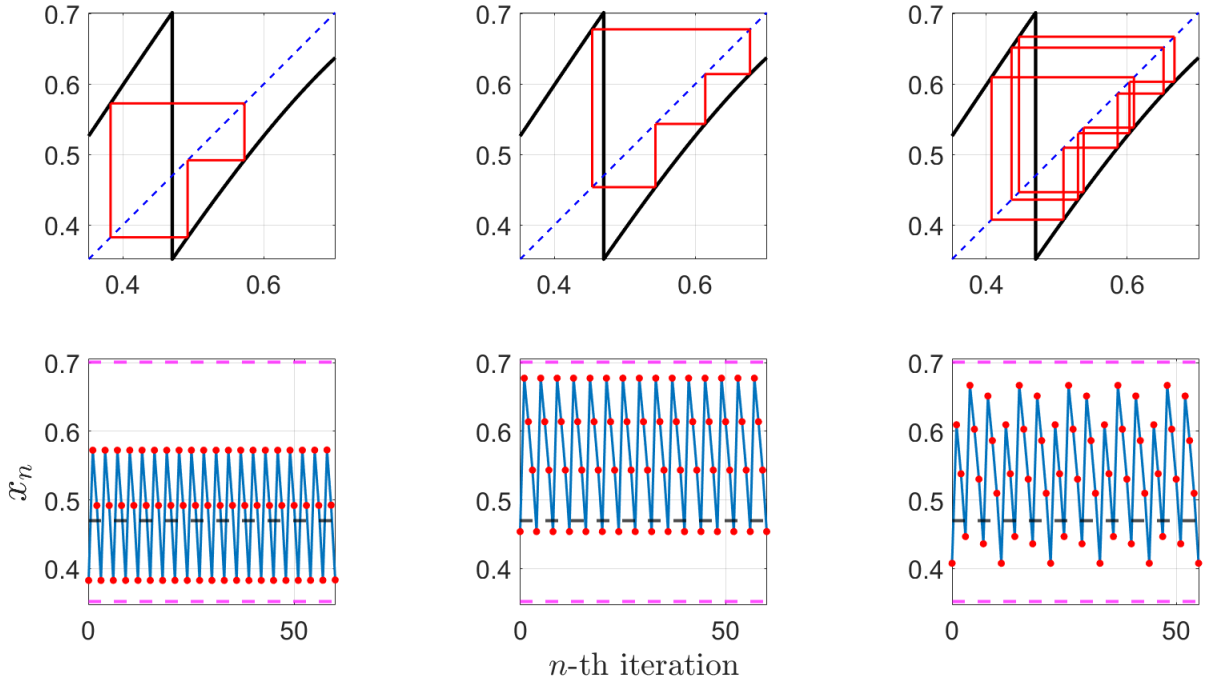

FIGURE 12. The fupo effect in the nlCNV system: creation of a periodic orbit of period 11 = 3 + 4 + 4 (right panel) from two periodic orbits of periods 3 and 4 (left and middle panels). The respective rotation numbers are Farey neighbours: $2/3 < 3/4$. Parameter values: $a = 0.1$, $d = 0.47$, $\alpha = -0.082$, $\beta = 0.35$, $\mu = 1.62$.

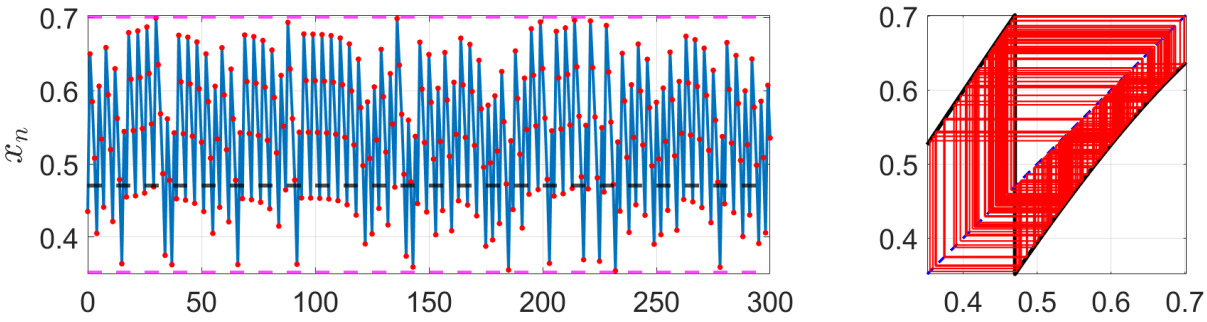

FIGURE 13. Chaotic spiking typical for the 1D nlCNV model: time series (left) and cobweb (right). Parameter values as in Figure 12. Initial point: $x_0 = 0.435$.

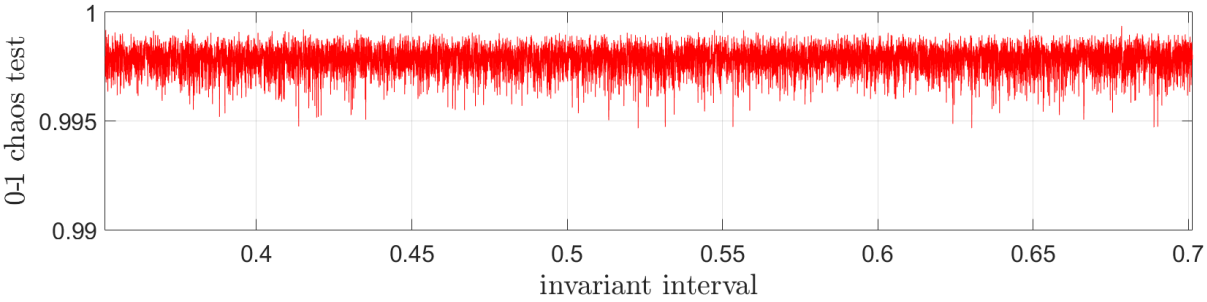

FIGURE 14. Results of 0-1 chaos test on the whole invariant interval $[b, c] = [0.35, 0.7]$ for 10^4 uniformly distributed initial points. The value of chaos test is very close to 1, which confirms chaotic behaviour of a randomly selected point in $[b, c]$. Parameter values of the model as in Figure 12.

MOST WIEDZY Downloaded from mostwiedzy.pl

implies that we can expect transient spiking behaviours which look like periodic ones (corresponding to initial conditions close to periodic orbits with given itineraries). Of course, numerically every such a "periodic orbit" will eventually "desynchronise" and the asymptotic behaviour observed will be irregular, but long transient periodic spiking patterns can be observed (as depicted in Figure 12).

6.2. **Examples and simulations.** In the last subsection we present results of numerical simulations related to the existence of periodic orbits with the specific periods in the 1D nlCNV model. They are conducted using MATLAB scripts, implementing fupo- and rotation theory of Lorenz-like maps and available in open repositories [4] and [5]. For convenience we denote here itineraries of periodic orbits by 0-1 sequences, instead of *L*-*R* sequences (i.e. 0 and 1 replace, respectively, *L* and *R* in encoding periodic orbits). Moreover, let a^i denote the repetition of the symbol or string a for i times.

TABLE 3. Concatenations of Farey neighbours itineraries with respect to α (other parameters: $\mu = 1.6$, $\beta = 0.455$, $a = 0.1$, $d = 0.37$).

α	rotation interval	Farey neighbours itineraries	Concatenations of 2nd and 3rd order
-0.25	$[0.888, 1]$	$8/9: 01^8$ $9/10: 01^9$	2nd: 01^801^9 3rd: $01^801^801^9$, $01^801^901^9$
-0.2	$[0.666, 0.8]$	$2/3: 01^2$ $3/4: 01^3$	2nd: 01^201^3 3rd: $01^201^201^3$, $01^201^301^3$
-0.15	$[0.5, 0.666]$	$1/2: 01$ $3/5: (01)^21$	2nd: $(01)^31$ 3rd: $(01)^41$, $(01)^31(01)^21$
-0.13	$[0.5, 0.555]$	$1/2: 01$ $6/11: (01)^51$	2nd: $(01)^61$ 3rd: $(01)^71$, $(01)^61(01)^51$

TABLE 4. Concatenations of Farey neighbours itineraries with respect to μ (other parameters: $\alpha = -0.065$, $\beta = 0.455$, $a = 0.1$, $d = 0.37$).

μ	rotation interval	Farey neighbours itineraries	Concatenations of 2nd and 3rd order
1.1	$[0.2, 0.25]$	$1/5: 10^4$ $1/4: 10^3$	2nd: 10^310^4 3rd: $10^310^310^4$, $10^310^410^4$
2.2	$[0.333, 0.5]$	$1/3: 10^2$ $1/2: 10$	2nd: 1010^2 3rd: $(10)^210^2$, 1010^210^2
2.75	$[0.357, 0.666]$	$2/5: (10)^20$ $1/2: 10$	2nd: $(10)^30$ 3rd: $(10)^40$, $(10)^30(10)^20$
3.1	$[0.5, 0.875]$	$1/2: 01$ $2/3: 011$	2nd: $(01)^21$ 3rd: $(01)^31$, $(01)^21011$

The Tables 3 and 4 depict the output of our MATLAB scripts for several parameters settings. We restrict ourselves to presenting only second and third order concatenations, because higher order concatenations become much longer. Let us describe briefly how our program works. First, we compute the rotation interval of a given 1D nlCNV map. Then we find inside the rotation interval the longest subinterval which endpoints are Farey neighbours. Note that the longest subinterval provides Farey neighbours with the smallest denominators and, in consequence, fupo with the shortest periods of periodic orbits. Finally, we construct

(1) finite periodic parts of the itineraries corresponding to these Farey neighbours according to the formula from Remark F.4) (denote these parts (blocks) by A and B),
(2) all concatenations of A and B of a given order n, i.e., formed by taking n blocks (each of them is A or B) concatenating all of them (see Theorem F.10).

MOST WIEDZY Downloaded from mostwiedzy.pl

Recall that the main idea behind fupo is that each Farey neighbours pair in the rotation interval guarantees the existence of infinitely many periodic orbits with itineraries being finite concatenations of itineraries corresponding to Farey neighbours. In other words, some distinguished pairs of periodic orbits (fupo) act as a machine producing infinitely many new periodic orbits with periods being the sum of multiples of the periods of the original pair. Moreover, each of such produced periodic orbits has unique itinerary determined by itineraries of fupo.

A quick analysis of the tables shows that, as could be expected,

- shorter rotation intervals produce longer periods and vice versa,
- the length of periods (related to the length of rotation intervals) does not change monotonically as the parameter increases.

Finally, observe that finite concatenations of itineraries represent a quite regular (although usually nonperiodic) type of finite binary sequences. For example, their Lempel-Ziv complexity (known as a good measure of the repetitiveness of binary sequences, see [41]) is low in comparison with random finite sequences, but we will not prove that fact here.

7. Activity patterns in the model

Our study of the 1D nlCNV model revealed that as a discrete dynamical system it certainly possesses very interesting dynamics that depends on a couple of parameters. However, since it originated from a neuron model, it is tempting to ask whether it can be viewed as a simple independent neuron model. For this purpose, let us consider the system:

$$x_{n+1} = \begin{cases} f(x_n) - y_n, & \text{if } x_n < d \\ f(x_n) - y_n - \beta, & \text{if } x_n \geq d, \end{cases} \tag{12}$$

where y_n can be treated as an external input current, constant or time-dependent. To emphasize that y can vary with time we write $y_n := \alpha(n)$, where $\alpha(n)$ is some function of time step n, independent of the value of x_n. This is partially in accordance with the original CNV model (4a)-(4b), where the external stimulus J is included only in the equation for the recovery variable y and changes the membrane voltage x indirectly through y. As previously, we refer to the system (12) as the 1D nlCNV. Note that in (12) the variable y enters the system with negative sign, i.e. the input current $y > 0$ acts as an inhibitory current whereas $y < 0$ would have an excitatory effect (we used this convention in our simulations below).

7.1. **Autonomous 1D nlCNV model.** Although studying the 1D nlCNV map $g(x)$ is mainly motivated by the need to explain the behaviour of the whole slow-fast 2D system (4a)-(4b), it appears that the 1D nlCNV model has surprisingly rich dynamics, even in the autonomous case when the input current $y = \alpha$ is constant. For example, in previous section we showed how the combinatorial structure of periodic orbits of the 1D nlCNV map can be matched with the spiking patterns generated. The real strength of the fupo-method used for this purpose is that it allows one to rigorously prove the existence of infinitely many periodic firing patterns of the 1D CNV model, which otherwise would be very hard to find numerically. In numerical simulations these patterns are not likely to persist asymptotically (due to the instability of periodic orbits) but, being aware of their existence, one can find initial conditions with long transient behaviour of the particular period and itinerary type. This also reveals a special feature of the 1D CNV model, where (unless the map g has an attracting fixed point as in Figure 3 in [17]) for wide range of parameters we are in expanding Lorenz map regime and asymptotic behaviour is always chaotic. Note that this makes the CNV model different than, for example, Chialvo model where in both 1D and 2D case (see [15, 42, 53]) asymptotically periodic behaviour could be observed due to the existence of attracting periodic orbits.

The 1D nlCNV model can display a great variety of behaviours under the constant stimulus current. Some of them are depicted in Figure 15, where we see chaotic bursting (top), tonic spiking (middle) or oscillatory spiking (bottom), which (depending on how one defines spikes) could

MOST WIEDZY Downloaded from mostwiedzy.pl

be also interpreted as subthreshold oscillations alternating with spikes (sort of mixed-mode oscillations). The corresponding value α of the external current and the values of other parameters are given in the figure's caption. We also include the value of the initial point. However, as we examined numerically, the qualitative behaviour rather did not depend on the initial point. Corresponding trajectories in the form of the cobweb plot are presented in Figure 16. We see clear matching between the orbit itineraries and distribution of points with the type of voltage trace in Figure 15 (for picture's clarity we include only parts of corresponding trajectories in the cobweb plots).

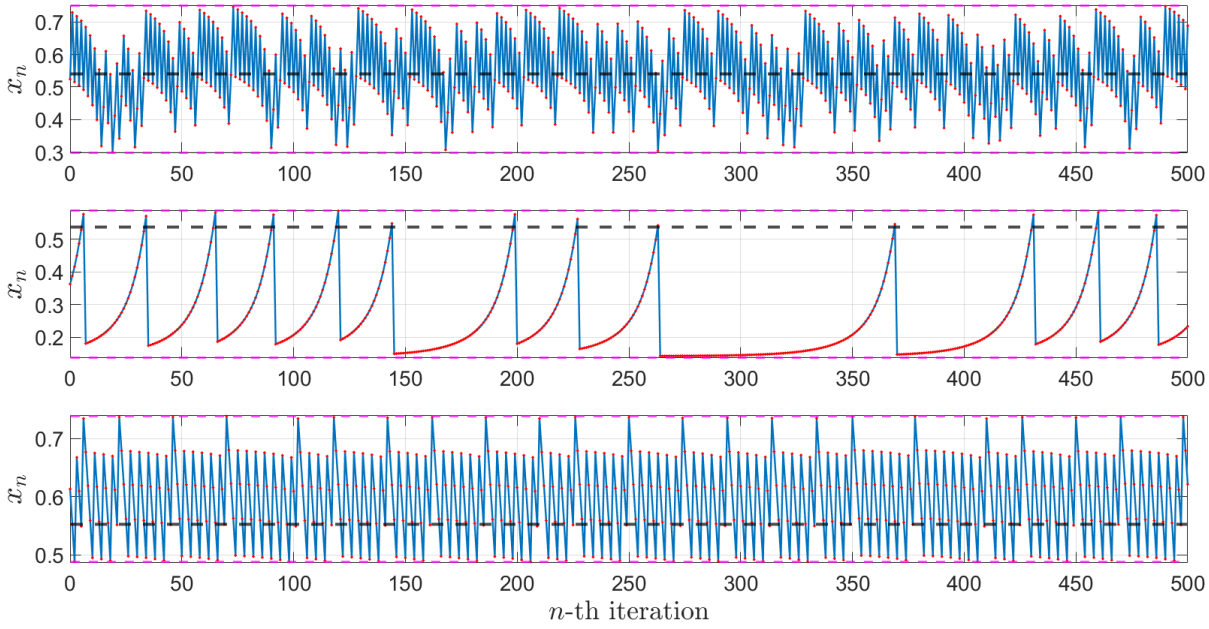

FIGURE 15. Three different patterns of time series reproducing consecutively from the top: bursting, tonic spiking and oscillatory spiking. Parameter values TOP: $\mu = 1.5, a = 0.15, d = 0.539, \alpha = -0.065, \beta = 0.45$, $x_0 = 0.524$; MIDDLE: $\mu = 0.5, a = 0.15, d = 0.539, \alpha = -0.0005, \beta = 0.45$, $x_0 = 0.363$; BOTTOM: $\mu = 0.405, a = 0.2, d = 0.553, \alpha = -0.15, \beta = 0.25$, $x_0 = 0.613$ (x_0 initial point). The horizontal dashed black line shows the discontinuity level.

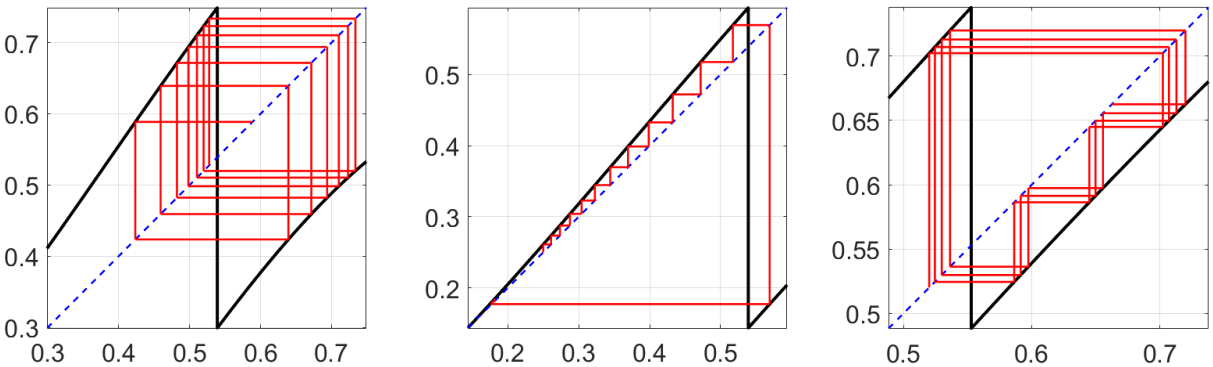

FIGURE 16. Three cobwebs for plots of the nlCNV maps corresponding (from the left) to the time series (from the top) presented on Figure 15. Parameter values as on this figure.

Note that stable periodic orbits might exist in the 1D nlCNV model beyond the expanding regime, studied by us herein. However, the absence of stable periodic behaviour and the presence of chaos

MOST WIEDZY Downloaded from mostwiedzy.pl

in the expanding case is not necessarily the disadvantage of the model as there are many map-based models especially designed to display chaotic behaviour such e.g. famous chaotic Rulkov model ([58]). On the other hand, chaotic spike trains appear commonly in experimental data, especially at the level of single cells (see e.g. [39] and references therein).

7.2. **Dynamics for varying input currents.** As we mentioned, the 2D CNV model can be seen as a slow-fast system with y as a slow variable which also depends on the external input J. However, the way at which the slow parameter y changes with time steps n has important implications. In particular, the works [44] and [45] numerically studied the one dimensional map (4a) with cubic function $F(x)$ when parameter $y = \alpha_n$ changes linearly and, respectively, sinusoidally with consecutive time instances $n = 1, 2, \ldots$. Their results on the transient chaotic dynamics in the 1D system (4a) with varying control parameter α_n suggest that even numerical analysis of chaotic dynamics in the 2D system (4a)-(4b) can be quite challenging. This is in correspondence with our results from Section 6 showing that even with constant input y the dynamics of trajectories shows variety of transiently-periodic behaviour, prior to the irregular, chaotic asymptotic behaviour. Similarly, numerical simulations presented in Figure 15 reveal that 1D model displays wide repertoire of different voltage traces that might be interpreted in terms of biological neurons behaviours, indicating that the intrinsic dynamics of such a neuron is very rich.

Motivated by this and the observations of other authors mentioned above, we now investigate the dynamics of the 1D nlCNV model under varying external input y since the way a neuron responses to a certain input is its most important property. For this purpose we consider two quite typical types of inputs: a periodic piecewise constant current with alternating stimulus amplitudes $y = \alpha_1$ and $y = \alpha_2$ and a constant stimulus with a short impulse of a larger amplitude. The results are presented, respectively, in Figure 17 and 18.

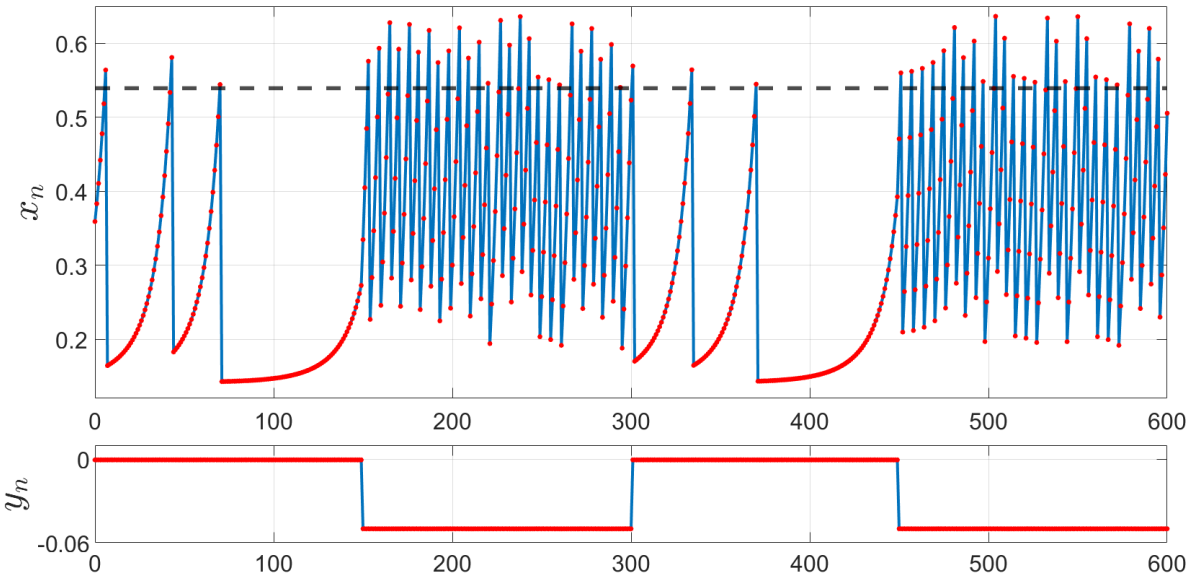

FIGURE 17. Alternate spiking and bursting as an effect of switching the values of $y = \alpha$ between y_1 and y_2. Other common parameter values of the 1D nlCNV model: $\mu = 0.49, a = 0.15, d = 0.539, \beta = 0.45, \alpha_1 = -0.0005, \alpha_2 = -0.05$. Initial point $x_0 = 0.359$. Each switchover takes place after 150 time units. The horizontal dashed black line shows the discontinuity level.

We see that periodically changing the value of the input current can cause switching between tonic spiking and bursting whereas the short impulse of higher amplitude changes temporarily the amplitude and frequency of oscillations. In fact even after removing the short impulse returning to the steady-behaviour might not be immediate and takes significant time. Note that as in our

MOST WIEDZY Downloaded from mostwiedzy.pl

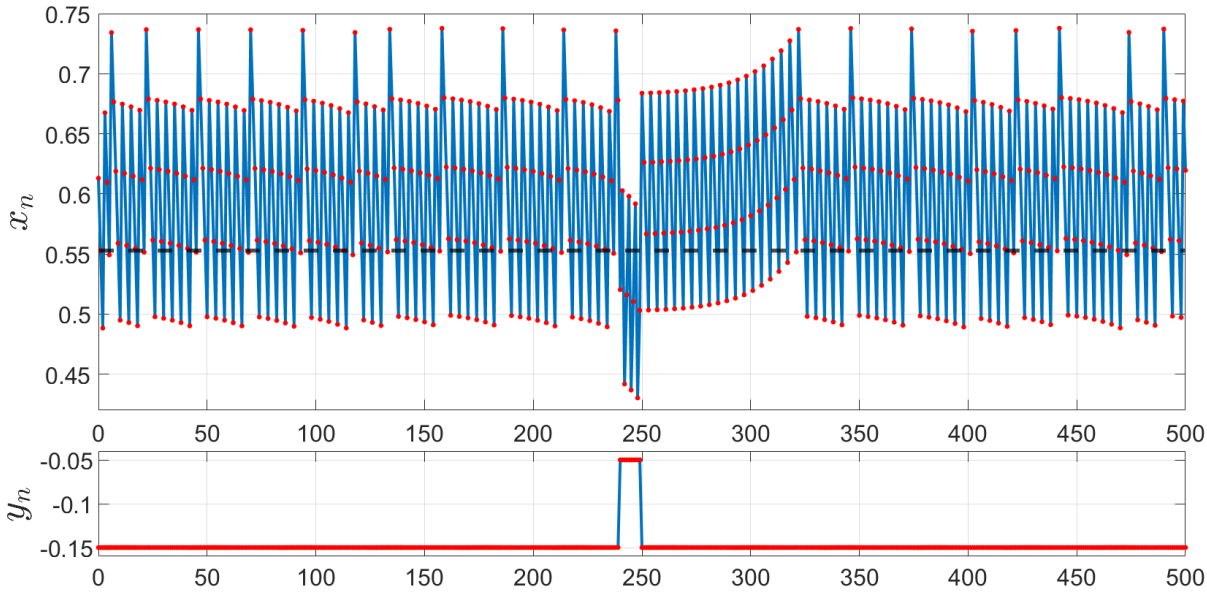

FIGURE 18. Transient adaptation of a spiking pattern as an effect of a short impulse of $y = \alpha$ in the 1D nlCNV model. Parameter values: $\mu = 0.405, a = 0.2, d = 0.55, \beta = 0.25, \alpha_1 = -0.15, \alpha_2 = -0.05$. Initial point $x_0 = 0.6131$. The horizontal dashed black line shows the discontinuity level.

convention the current y has an inhibitory role, applying current with greater (or less negative) amplitude in general results in smaller potential values and lower frequency of oscillations.

7.3. **Multistability.** Figure 18 depicts a situation when a short impulse of a different amplitude has only temporal effect on the neuron's voltage trace since after removing the impulse the system returns to its previous behaviour. But this is not always the case. In particular, in Figure 20 the neuron is firstly subjected to a constant input with amplitude of α_1 under which it converges to a resting state. However, applying an inhibitory current of the amplitude α_2 (for some duration time) causes firstly a rapid increase in voltage and small oscillations (bursting). Next the input level returns back to α_1 but the neuron does not return to its previous resting state. Instead, it generates chaotic spiking oscillations. This phenomena can be explained by looking at the left panel of Figure 19 which shows the map g obtained for $y = \alpha_1$ and the same values of other parameters. The map features two fixed points, stable and unstable, with stable fixed point corresponding to the resting state. But initial conditions to the right of the unstable fixed point get trapped within the invariant interval (marked as a red square). Therefore applying additional inhibition to the neuron converging to its resting state shifts the graph of g up and enables "escaping" from the basin of attraction of the stable fixed point (or disappearance of the fixed points as a result of saddle-node bifurcation). If that inhibition is within a proper range of amplitudes and its duration is not too short nor too long, then after removing the inhibitory pulse, the graph of g returns to its initial configuration but the trajectory stays constrained in the invariant interval exhibiting chaotic spiking (or chaotic subthreshold oscillations, depending on the interpretation). Therefore even a transient input current can control switching between various oscillatory modes and detailed explanation of these effects can be a subject of further studies.

For completeness we also notify that fixed points can appear to the right of the discontinuity point, with a particular example on the right panel of Figure 19.

7.4. **Shape of an action potential.** Obviously, in case of a simple 1D map-based model, we do not aim at reproducing real time-continuous voltage recordings of biological neurons. However, expecting such a good matching with the real data is usually also not possible with higher dimensional discrete models or often even for their ODE- or hybrid counterparts. Rather, for map-based

MOST WIEDZY Downloaded from mostwiedzy.pl

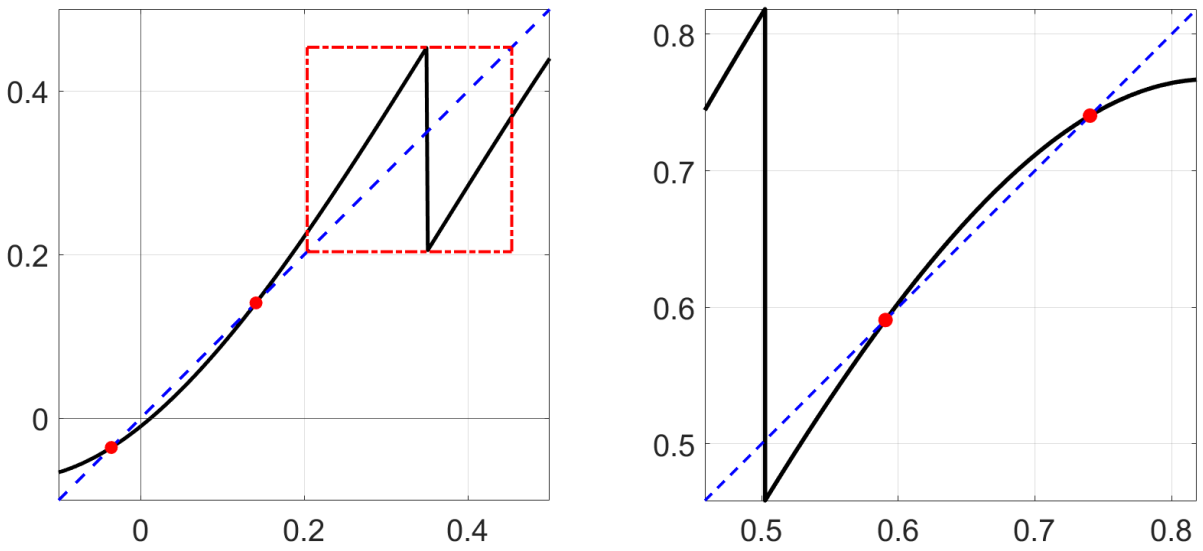

FIGURE 19. Stable and unstable fixed points (red dots) of two 1D nlCNV maps. On the left panel both points outside the invariant interval (red square). On the right panel inside the invariant interval. Parameter values: LEFT $\mu = 2, a = 0.1, d = 0.35, \alpha = 0.01, \beta = 0.25$; RIGHT $\mu = 2.55, a = 0.01, d = 0.5025, \alpha = -0.002, \beta = 0.36$.

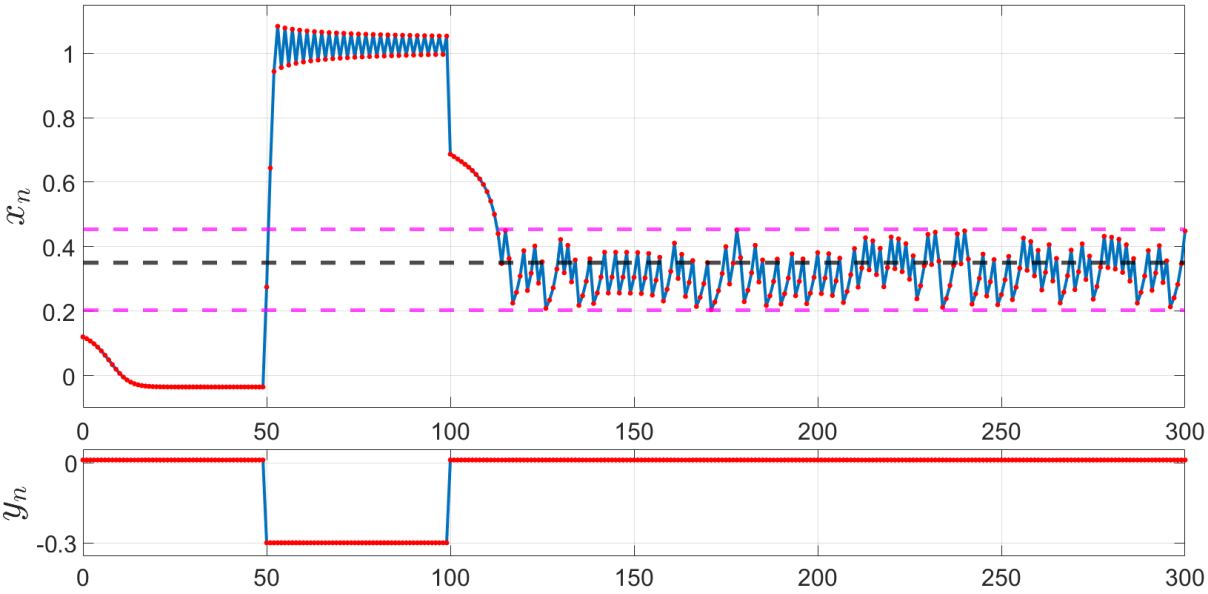

FIGURE 20. Switching between various stable modes as an effect of an impulse of $y = \alpha$ in the 1D nlCNV model. Parameter values: $\mu = 0.2, a = 0.1, d = 0.35, \beta = 0.25, \alpha_1 = 0.01, \alpha_2 = -0.3$. Initial point $x_0 = 0.12$. The horizontal dashed black line shows the discontinuity level and horizontal dashed maroon lines range of invariant interval corresponding to α_1.

models we are interested in reproducing the general spike train pattern (such as e.g. tonic spiking, subthreshold oscillations, chaotic bursting etc.) and sometimes just the information on whether in a given interval there was a spike or what is the average firing rate. From that point of view the 1D nlCNV model shows quite surprising ability to mimic various neuronal behaviours, some of them presented above. The reason for that is two-fold: firstly, in the discrete setting complex dynamics (e.g. chaos) can arise even in one dimension and, secondly, the discontinuity present in

MOST WIEDZY Downloaded from mostwiedzy.pl

the system allows for new types of behaviours not present in continuous maps, yet maintaining the complexity of e.g. unimodal continuous map.

An interesting feature of the 1D nlCNV model is that, even under constant stimulus, it is possible to reconstruct various shapes of action potential. One shape of an action potential is visible in the middle panel of Figure 15, where the voltage firstly slowly increases, then depolarization accelerates and finally the voltage rapidly drops down. This is in correspondence with the trajectory that features many consecutive iterates on the left of the discontinuity point, followed by a point on the right and then turning to the left side again, as visible in the middle panel of Figure 16. This configuration is likely among trajectories with rotation numbers of the form $1/q$, where q is large, as follows from the definition of the rotation number. On the other hand, Figure 21 presents an action potential where depolarization of the membrane voltage is very rapid whereas repolarization (decrease in the membrane voltage) takes many time instances and has a different shape. Such a shape corresponds to the so-called cardiac action potential which has been recently reported in Hindmarsh–Rose model as well as in the logistic KTz model in autonomous regime ([7]). Therefore KTz model model is another example of a map-based model which can successfully reconstruct dynamical behaviour present in more complicated higher dimensional continuous-time models. Interestingly, cardiac spikes are also present in the 1D nlCNV model and are realized by trajectories featuring a point to the left of the discontinuity point alternating with a series of points to the right of the discontinuity, as depicted in the right panel of Figure 21 which presents a couple of initial points on such a trajectory. This, in turn, is likely to occur for trajectories with rotation numbers of the form $(q-1)/q$, where q is relatively large. It also seems that it is the discontinuity and in particular Lorenz-like nature of the 1D nlCNV map that enables generating cardiac-like and 'typical' spikes.

Remark 7.1. The voltage trace of cardiac-like spikes depicted in Figure 21 has been obtained for the 1D nlCNV model beyond the expanding Lorenz map regime (since the infimum of the derivative g' is slightly less than 1). However, the map is still Lorenz-like.

The above remark suggests than studying the nlCNV model beyond the expanding case is also of interest. Nevertheless we also expect that it is possible to obtain a similar shape of spikes for expanding Lorenz map, e.g. with infimum of derivative slightly greater than 1. In addition, it is worth pointing out the following two observations.

Remark 7.2. If the map g in the 1D nlCNV model is expanding (in the invariant interval of interest), then all the orbits (with initial condition in this interval) are unstable. However, for non-expanding maps (such as in Figure 21) it makes sense to study stability of the periodic orbits.

Remark 7.3. In both situations of various types of action potentials such as in the middle panel of Figure 15 and in Figure 21 we are in the vicinity of the "ghost" of the fixed point (see corresponding cobwebs) which makes the trajectories move slowly and very close to the diagonal. In purely expanding Lorenz map setting (i.e. under conditions listed in Table 1), fixed points are not possible in the invariant interval but adjusting parameters beyond this regime enables this as well as non-overlapping setting where stable periodic behaviour exists.

In the current work we focus mainly on the expanding case (motivated by the presence of clear chaotic behaviour) but the above remarks, results of simulations and observations suggest that obtaining comprehensive picture of the dynamics in the whole multidimensional parameter space of the 1D nlCNV map could be a subject for further research. Certainly, the behaviour of this, apparently simple, one dimensional discrete model is richer than, for example, for one dimensional IF models.

Discussion and conclusions

Let us briefly summarize the presented results and discuss some possibilities of further developments.

MOST WIEDZY Downloaded from mostwiedzy.pl

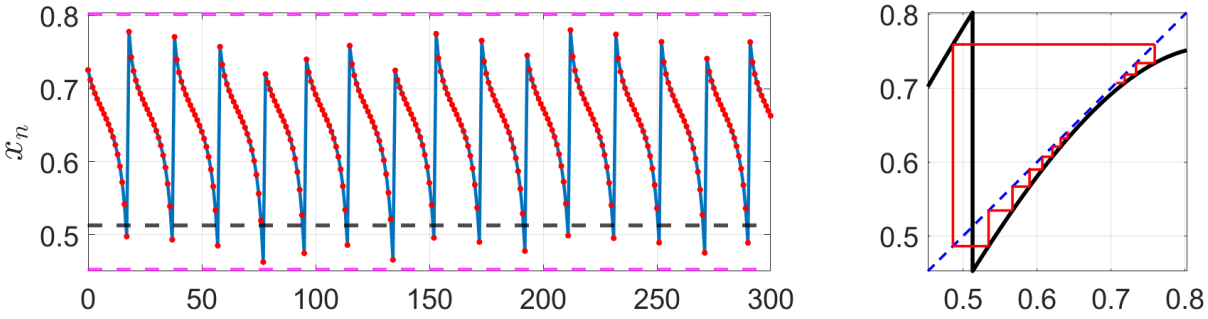

FIGURE 21. Cardiac spiking in the 1D nlCNV model (time series left, cobweb right). Parameter values: $\mu = 2.5, a = 0.05, d = 0.5127, \alpha = -0.0005, \beta = 0.35$. Initial point: $x_0 = 0.6271$.

Firstly, we have showed how chaos theory and rotation theory of Lorenz-like and expanding Lorenz maps, which main results we reviewed in the first section and in Appendix A, can be effectively applied to the study of the 1D nlCNV model. In particular, we have rigorously established sufficient conditions for the 1D nlCNV map to be an expanding Lorenz map on an appropriate invariant interval (Theorem 3.1) and showed that the set of parameters where these conditions are satisfied is "not small" (Theorem 3.2 and Proposition 3.3). Next, we directed our interests towards chaotic properties of the model by providing theoretical and more explicit conditions under which the 1D model exhibits chaos in the sense of Devaney on the whole invariant interval (Theorem 4.1 and Lemma 4.2, respectively). Then we investigated the range of chaotic behaviour in the α-β parameter plane (Theorem 4.3, Table 5 and plots in Figure 4). The even more fundamental properties of the model are its ergodicity and acip, which are related to the distribution of orbits. Depending on parameters (see Figure 5), a typical orbit can asymptotically accumulate on the whole invariant interval or on the union of its disjoint subintervals. Further, explicit conditions for the existence of period 2 orbit have been provided (Lemma 5.1 and Theorem 1.5) and numerical investigation of the behaviour of the rotation interval with respect to the various parameters have yield that, as expected, the endpoints of this interval typically depend monotonically on a given parameter but, interestingly, its length (which might be identified with a sort of complexity measure) might change in a far more complicated way. Finally, using the notion of fupos, we have matched the itineraries of periodic orbits and their concatenations with spike patterns fired for the 1D nlCNV model (Propositions 6.1 and 6.2). We also included further numerically obtained examples depicting the behaviour of the model established by some of our results, especially in terms of concatenations of periodic itineraries obtained from "most prominent" twist periodic orbits. However, as we have showed, the voltage traces produced by the 1D nlCNV model can be both irregular (i.e. non-periodic, "chaotic") or (transiently) periodic which might depend on the initial voltage value and be quite fragile to the small variation in parameters. The last section discusses biological relevance of the findings on the 1D nlCNV model and shows that even with constant external stimulus the 1D model can present variety of behaviours.

There arises though a natural question on the implications of these results for the original 2D nlCNV model. Note that due to the discrete, and discontinuous, nature of this model obtaining rigorous mathematical results (formal theorems and proofs) seems quite challenging and is an interesting topic for further research. However, since the 1D nlCNV model, which can be seen as a Poincaré section of the full model, already shows significant complexity (e.g. in terms of spiking patterns fired as established by Propositions 6.1 and 6.2), we can expect that the level of complexity of the full 2D model is not less than that of its 1D reduction and thus providing the results on the 2D system, maintaining the same level of analytical rigorousness, is very challenging. In fact, the first steps in the direction of rigorous examination of the 2D model, are the results concerning behaviour of the 1D reduction with respect to the α-parameter (since this parameter corresponds to the y-variable in the 2D model), in particular our Theorems 3.2, 1.5 and 4.3 since, as also

MOST WIEDZY Downloaded from mostwiedzy.pl

pointed out in [17], the dynamical mechanism of chaotic behaviour in the 2D model is induced by the 1D nlCNV map.

Another idea comes by applying elements of fast-slow analysis since with $\varepsilon \to 0$ the 2D model shows a natural separation of time scales in which case y becomes a slow parameter controlling the evolution of the voltage x. Observations in this vein were included in the main works on the CNV model ([17, 18]). Nevertheless, the rigorous approach would require applying the tools of discrete geometric singular perturbation theory as recently developed in [34] and illustrated therein, among others, with the example of the Chialvo model ([15]), where some parameter sets corresponding to various types of spiking dynamics could be identified. Unfortunately, the 1D CNV map is not continuous, contrary to the map describing the evolution of the voltage variable x in the Chialvo model, which seems to be a technical obstacle in such analysis.

Acknowledgements. Frank Llovera Trujillo and Justyna Signerska-Rynkowska were supported by NCN (National Science Centre, Poland) grant no. 2019/35/D/ST1/02253. Justyna Signerska-Rynkowska also acknowledges the support of Dioscuri program initiated by the Max Planck Society, jointly managed with the National Science Centre (Poland), and mutually funded by the Polish Ministry of Science and Higher Education and the German Federal Ministry of Education and Research.

Authors' Declarations

Conflict of Interest. The authors have no conflicts to disclose.

Author Contributions. Piotr Bartłomiejczyk:

Conceptualization (equal); Data curation (lead); Formal analysis (equal); Investigation (equal); Methodology (equal); Resources (equal); Software (equal); Supervision (equal); Validation (equal); Visualization (equal); Writing – original draft (equal); Writing – review & editing (equal).

Frank Llovera Trujillo

Data curation (equal); Formal analysis (equal); Investigation (equal); Software (lead); Visualization (equal); Validation (equal); Writing – original draft (equal).

Justyna Signerska-Rynkowska:

Conceptualization (equal); Formal analysis (equal); Funding acquisition (lead); Investigation (equal); Methodology (equal); Supervision (equal); Validation (equal); Writing – original draft (equal); Writing – review & editing (equal).

Data Availability. The data (software) upon which our numerical computations are based is publicly and freely available at [4] and [5].

References

[1] C. Aguirre, D. Campos, P. Pascual, E. Serrano, *Neuronal behaviour with sub-threshold oscillations and spiking/bursting activity using a piecewise linear two-dimensional map*, in: Artificial Neural Networks: Biological Inspirations ICANN 2005, Springer, Berlin, Germany, 2005, pp. 103–108

[2] L. Alsedà, J. Llibre, M. Misiurewicz, C. Tresser, *Periods and entropy for Lorenz-like maps* Ann. Inst. Fourier (Grenoble) **39**, 1989, 929–952.

[3] V. I. Arnold, *Cardiac arrhythmias and circle mappings* Chaos **1**, 1991, 20–24.

[4] P. Bartłomiejczyk, F. Llovera Trujillo, J. Signerska-Rynkowska, *FUPOlibrary*, `https://www.mathworks.com/matlabcentral/fileexchange/135937-fupolibrary`, MATLAB Central File Exchange, 2023. Retrieved September 27, 2023.

[5] P. Bartłomiejczyk, F. Llovera Trujillo, J. Signerska-Rynkowska, *FUPOlibrary*, `https://github.com/bartlomiejczyk/FUPOlibrary`, GitHub repository, 2023. Retrieved September 27, 2023.

[6] P. Bartłomiejczyk, F. Llovera-Trujillo, J. Signerska-Rynkowska, *Spike patterns and chaos in a map-based neuron model*, Int. J. Appl. Math. Comput. Sci. **33**, 2023, 395–408

[7] G. S. Bortolotto, R. V. Stenzinger, M. H. R. Tragtenberg, *Electromagnetic induction on a map-based action potential model.*, Nonlinear. Dyn. **95**, 2019, 433–444.

[8] A. Boyarsky, P. Góra, *Laws of chaos. Invariant measures and dynamical systems in one dimension*, Probability and its Applications Birkhäuser Boston, Inc., Boston, MA, 1997.

[9] R. Brette, *Dynamics of one-dimensional spiking neuron models.*, J. Math. Biol. **48**, 2004, 38–56.

MOST WIEDZY Downloaded from mostwiedzy.pl

[10] R. Brette, W. Gerstner, *Adaptive exponential integrate-and-fire model as an effective description of neuronal activity*, J. Neurophysiol. **94**, 2005, 3637–3642.
[11] H. Bruin, *Topological and Ergodic Theory of Symbolic Dynamics*, American Mathematical Society, 2023.
[12] N. Brunel, M.C. van Rossum, *Lapicque's 1907 paper: from frogs to integrate-and-fire.*, Biol Cybern. **97**, 2007, 337–339.
[13] H. Carrillo, F. Hoppensteadt, *Unfolding an electronic integrate-and-fire circuit*, Biol. Cybern., **102**, 2010, 1–8.
[14] B. Cazelles, M. Courbage, M. Rabinovich, *Anti-phase regularization of coupled chaotic maps modelling bursting neurons*, Europhysics Letters, **56**, 2001, 504.
[15] D. R. Chialvo, *Generic excitable dynamics on a two-dimensional map*, Chaos Solitons Fractals **5**(3–4), 1995, 461–479.
[16] S. Coombes, P. Bresslof, *Mode locking and Arnold tongues in integrate-and-fire oscillators*, Phys. Rev. E, **60**, 1999, 2086–2096.
[17] M. Courbage, V. I. Nekorkin, L. V. Vdovin, *Chaotic oscillations in a map-based model of neural activity*, Chaos **17**, 043109, 2007.
[18] M. Courbage, V. I. Nekorkin, *Map based models in neurodynamics* Int. J. Bifurcation Chaos **20**, no. 06, 2010, 1631–1651.
[19] M. Courbage, O. V. Maslennikov, V. I. Nekorkin, *Synchronization in time-discrete model of two electrically coupled spike-bursting neurons*, Chaos Solitons Fractals **45**, no. 05, 2012, 645–659.
[20] R. FitzHugh, *Mathematical models of the threshold phenomena in the nerve membrane.*, Bull. Math. Biophys. **17**, 1955, 257–278.
[21] R. FitzHugh, *Impulses and physiological states in theoretical models of nerve membrane.*, Biophysical J. **1**, 1961, 445–466.
[22] T. Gedeon, M. Holzer, *Phase locking in integrate-and-fire models with refractory periods and modulation.*, J. Math. Biol. **49**, 2004, 577–603.
[23] W. Geller, M. Misiurewicz, *Farey-Lorenz permutations for interval maps*, Int. J. Bifurcation Chaos, **28** (2018), 1850021 (7 pages).
[24] L. Glass, *Synchronization and rhythmic processes in physiology.*, Nature, **410** (2001), 277–284.
[25] G. A. Gottwald, I. Melbourne, *The 0-1 Test for Chaos: A Review.*, In: Skokos, C., Gottwald, G., Laskar, J. (eds) Chaos Detection and Predictability. Lecture Notes in Physics, **915**, Springer, Berlin, Heidelberg, 2016.
[26] A. Granados, L. Alsedà, M. Krupa, *The Period adding and incrementing bifurcations: from rotation theory to applications*, SIAM Review, 2017, **59**(2), 225–292.
[27] A. Hess, L. Yu, I. Klein, M. De Mazancourt, G. Jebrak, et.al., *Neural Mechanisms Underlying Breathing Complexity.*, PLoS ONE **8**(10), 2013, e75740.
[28] J. L. Hindmarsh, R. M. Rose, *A model of neuronal bursting using three coupled first order differential equations*, Proc. R. Soc. Lond. B., **221**, 1984, 87–102.
[29] A. L. Hodgkin, A. F. Huxley, *A quantitative description of membrane current and its application to conduction and excitation in nerve.*, The Journal of Physiology **117**, 1952, sp004764.
[30] B. Ibarz, J. M. Casado, M. A. F. Sanjuán, *Map-based models in neuronal dynamics*, Phys. Rep. **501**(1–2), 2001, 1–74.
[31] E. M. Izhikevich, *Simple model of spiking neurons*, IEEE Trans. Neural Netw. **14**, 2003, 1569–1572.
[32] E. M. Izhikevich, F. Hoppensteadt, *Classification of bursting mappings*, International Journal of Bifurcation and Chaos **14**, 2004, 3847–3854.
[33] J. Jaquette, S. Kedia, E. Sander, J.D. Touboul, *Reliability and robustness of oscillations in some slow-fast chaotic systems*, Chaos: An Interdisciplinary Journal of Nonlinear Science **33**, 2023, 103135.
[34] S. Jelbart, C. Kuehn, *Discrete geometric singular perturbation theory*, Discrete Contin Dyn Syst Ser A **43**(1), 2023, 57–120.
[35] A. Kameyama, *Topological transitivity and strong transitivity*, Acta Math. Univ. Comenianae (N.S.) **71**(2) (2002), 139–145.
[36] P. Kasprzak, A. Nawrocki, J. Signerska-Rynkowska, *Integrate-and-fire models with an almost periodic input function*, Journal of Differential Equations **264** (2018), 2495–2537.
[37] A. Katok, B. Hasselblatt, *Introduction to the Modern Theory of Dynamical Systems* (Encyclopedia of Mathematics and its Applications), Cambridge: Cambridge University Press, 1995.
[38] J. P. Keener, F. C. Hoppensteadt, J. Rinzel, *Integrate-and-Fire Models of nerve membrane response to oscillatory input*, SIAM J. Appl. Math **41** (1981), 503–517.
[39] H. Korn, Ph. Faure, *Is there chaos in the brain? II. Experimental evidence and related models*, Comptes Rendus Biologies **326** (2003), 787–840.
[40] L. Lapicque, *Recherches quantitatives sur l'excitation électrique des nerfs traitée comme une polarisation*, J. Physiol. Pathol. Gen., **9**, 1907, 620–635.
[41] A. Lempel, J. Ziv, *On the Complexity of Finite Sequences*, IEEE Trans. on Information Theory, **22**(1), 1976, 75–81.
[42] F. Llovera-Trujillo, J. Signerska-Rynkowska, P. Bartłomiejczyk, *Periodic and chaotic dynamics in a map-based neuron model*, Math. Meth. Appl Sci. **46**, 2023, 11906–11931.

MOST WIEDZY Downloaded from mostwiedzy.pl

[43] O. V. Maslennikov, V. I. Nekorkin , *Discrete model of the olivo-cerebellar system: structure and dynamics*, Radiophys. Quantum El. **55**(3), 2012, 198–214.
[44] O. V. Maslennikov, V. I. Nekorkin , *Dynamic boundary crisis in the Lorenz-type map*, Chaos **23**, 2013, 023129.
[45] O. V. Maslennikov, V. I. Nekorkin, J. Kurths, *Transient chaos in the Lorenz-type map with periodic forcing*, Chaos **28**(3), 2018, 033107.
[46] M. Misiurewicz, *Rotation intervals for a class of maps of the real line into itself*, Ergodic Theory and Dynamical Systems **6**(1), 1986, 117–132.
[47] C. Morris, H. Lecar, *Voltage oscillations in the barnacle giant muscle fiber.*, Biophys. J. **35**, 1981, 193–213.
[48] S. Newhouse, J. Palis, F. Takens *Bifurcations and stability of families of diffeomorphisms*, Inst. Hautes Études Sci. Publ. Math. **57**, 1983, 5–71.
[49] J. Nagumo, S. Arimoto, S. Yoshizawa *An active pulse transmission line simulating nerve axon.*, Proc IRE. **50**, 1962, 2061–2070.
[50] P. Oprocha, P. Potorski, P. Raith, *Mixing properties in expanding Lorenz maps*, Adv. Math. **343** (2019), 712–755.
[51] K. Pakdaman, *Periodically forced leaky integrate-and-fire model.*, Phys Rev E Stat Nonlin Soft Matter Phys. **63** (2001), 041907.
[52] A. Peris, *Transitivity, dense orbit and discontinuous functions.*, Bull. Belg. Math. Soc. Simon Stevin **6** (1999), 391–394.
[53] P. Pilarczyk, J. Signerska-Rynkowska, G. Graff, *Topological-numerical analysis of a two-dimensional discrete neuron model.*, Chaos. **33** (2023), 043110.
[54] D. Reyner-Parra, G Huguet, *Phase-locking patterns underlying effective communication in exact firing rate models of neural networks.*, PLoS Comput Biol **18** (2022), e1009342.
[55] F. Rhodes, Ch. L. Thompson, *Rotation Numbers for Monotone Functions on the Circle*, Journal of the London Mathematical Society s2, **34**(2), 1986, 360–368.
[56] J. E. Rubin, J. Signerska-Rynkowska, J. D. Touboul, A. Vidal, *Wild oscillations in a nonlinear neuron model with resets: (I) Bursting, spike-adding and chaos.*, Discrete and Continuous Dynamical Systems - B, **22**, 2017, 3967–4002.
[57] J. E. Rubin, J. Signerska-Rynkowska, J. D. Touboul, A. Vidal, *Wild oscillations in a nonlinear neuron model with resets: (II) Mixed-mode oscillations.*, Discrete and Continuous Dynamical Systems - B, **22**, 2017, 4003–4039.
[58] N. F. Rulkov, *Regularization of synchronized chaotic bursts*, Phys. Rev. Lett. **86**, 2001, 183–186.
[59] N. F. Rulkov, *modelling of spiking-bursting neural behaviour using two-dimensional map*, Phys. Rev. E **65**, 2002, 041922.
[60] A. L. Shilnikov, N. F. Rulkov, *Subthreshold oscillations in a map-based neuron model*, Phys. Lett. A **328**, 2004, 177–184.
[61] R. Smidtaite, M. Ragulskis, *Finite-time divergence in Chialvo hyperneuron model of nilpotent matrices*, Chaos, Solitons & Fractals **179**, 2024, 114482.
[62] J. Touboul, R. Brette, *Spiking dynamics of bidimensional integrate-and-fire neurons*, IAM J. Appl. Dyn. Syst. **8**, 2009, 1462–1506.
[63] L. Yu, M. De Mazancourt, A. Hess, *Functional connectivity and information flow of the respiratory neural network in chronic obstructive pulmonary disease.*, Hum Brain Mapp **37**, 2016, 2736–2754.
[64] Y. Yue, Y. J. Liu, Y. L. Song, Y. Chen, L. C. Yu, *Information Capacity and Transmission in a Courbage-Nekorkin-Vdovin Map-Based Neuron Model.*, Chin. Phys. Lett. **34**, 2017, 048701.

Appendix A. Theory of Lorenz-like maps

A.1. **Basic definitions.** Let (X, d) be a compact metric space and $f : X \to X$ a map (not necessarily continuous). Recall that a nonempty and open set $U \subset X$ is called *opene*.

We start with the following general notions.

Definition A.1. The map f is called

- *transitive* if for every two opene sets $U, V \subset X$ there is $n \in \mathbb{N}$ such that $f^n(U) \cap V \neq \emptyset$,
- *mixing* if for every two opene sets $U, V \subset X$ there is $N \in \mathbb{N}$ such that for every $n \geq N$ we have $f^n(U) \cap V \neq \emptyset$,
- *sensitive* if there exists a $\delta > 0$ such that for every $x \in X$ and every neighbourhood U of x, there exists $y \in U$ and $n \in \mathbb{N}$ such that $d(f^n(x), f^n(y)) > \delta$,
- *expansive* if there exists a $\delta > 0$ such that for any $x, y \in X$, $x \neq y$, there exists $n \in \mathbb{N}$ such that $d(f^n(x), f^n(y)) > \delta$.

We remark that

- mixing implies transitivity,

MOST WIEDZY Downloaded from mostwiedzy.pl

- expansiveness implies sensitivity.

One of the most classical definitions of chaos is due to R. L. Devaney.

Definition A.2. A map $f\colon X \to X$ is called *chaotic in the sense of Devaney* on X if

(1) f is transitive,
(2) the set of periodic points of f is dense in X,
(3) f is sensitive.

An interesting class of maps are Lorenz-like and expanding Lorenz maps, which are special type of maps defined on the subinterval of the real line, i.e. $X = [a, b] \subset \mathbb{R}$. Therefore next definitions and results will be formulated for $f : [0, 1] \mapsto [0, 1]$ (which naturally extends to the case $f\colon [a, b] \mapsto [a, b]$).

Definition A.3. We say that a map $f\colon [0, 1] \to [0, 1]$ is *strongly transitive* if for every nonempty open subinterval $J \subset (0, 1)$ there exists $n \in \mathbb{N}$ such that $\bigcup_{i=0}^{n} f^n(J) \supset (0, 1)$.

Note that strong transitivity implies transitivity. The opposite is, in general, not true, but the following essential result holds (see [35, Thm. 3]).

Theorem A.4. *Assume that $f\colon [0, 1] \to [0, 1]$ is piecewise continuous piecewise strictly monotone. If f is transitive then it is strongly transitive.*

Definition A.5. A *Lorenz-like map* is a map f of an interval $[0, 1]$ to itself, for which there exists a point $c \in (0, 1)$ such that

- f is continuous and increasing (not necessarily strictly) on $[0, c)$ and on $(c, 1]$,
- $\lim_{x\to c^-} f(x) = 1$ and $\lim_{x\to c^+} f(x) = f(c) = 0$.

The intervals of continuity in the domain of the Lorenz map play a crucial role in its analysis. Therefore denote $I_L = [0, c)$ and $I_R = [c, 1]$.

Definition A.6. The Lorenz-like map f is called *nonoverlapping* if $f(0) > f(1)$ (i.e. when $f(I_L) \cap f(I_R) = \emptyset$). Otherwise, (i.e. when $f(0) \leq f(1)$ implying $f(I_L) \cap f(I_R) \neq \emptyset$), the map is called *overlapping*.

It turns out that nonoverlapping and overlapping Lorenz-like maps have completely distinct properties (see e.g. [46, 55]), especially in terms of their rotation sets as mentioned in next subsection.

Definition A.7. An *expanding Lorenz map* is a map $f\colon [0, 1] \to [0, 1]$ satisfying the following three conditions:

- there is a *critical point* $c \in (0, 1)$ such that f is continuous and strictly increasing on $[0, c)$ and $(c, 1]$,
- $\lim_{x\to c^-} f(x) = 1$ and $\lim_{x\to c^+} f(x) = f(c) = 0$,
- f is differentiable for all points not belonging to a finite set $F \subset [0, 1]$ and such that $\inf\{f'(x) \mid x \in [0, 1] \setminus F\} > 1$.

Observe that expanding Lorenz maps are overlapping Lorenz-like maps. Moreover, every expanding Lorenz map is expansive (see [6, Prop. 1]).

A.2. **Chaos in Lorenz maps.** Let

$$f_1(x) = \sqrt{2}x + \frac{2 - \sqrt{2}}{2} \pmod 1,$$

$$f_2(x) = \sqrt[3]{2}x + \frac{2 + \sqrt[3]{4} - 2\sqrt[3]{2}}{2} \pmod 1,$$

$$f_3(x) = \sqrt[3]{2}x + \frac{2 - \sqrt[3]{4}}{2} \pmod 1$$

MOST WIEDZY Downloaded from mostwiedzy.pl

for $x \in [0,1]$.

The results for the occurrence of chaos and related phenomena in expanding Lorenz maps, important from the point of view of further analysis of the nlCNV model, can be summarized in the following:

Theorem A.8. *Let $f : [0,1] \to [0,1]$ be an expanding Lorenz map. Then the following conditions are equivalent:*

- *f is transitive*
- *f is strongly transitive*
- *f is chaotic in the sense of Devaney.*

Now let $\lambda := \inf\{f'(x) \mid x \in [0,1] \setminus F\}$. If one of the following conditions is satisfied:

(i) $\sqrt{2} \leq \lambda \leq 2$,
(ii) $\sqrt[3]{2} \leq \lambda < \sqrt{2}$ *and* $f(0) \geq \frac{1}{1+\lambda}$,
(iii) $\sqrt[3]{2} \leq \lambda < \sqrt{2}$ *and* $f(1) \leq 1 - \frac{1}{1+\lambda}$,

then f is chaotic in the sense of Devaney.

Moreover, if $f \neq f_1$, $f \neq f_2$ and $f \neq f_3$, then f is also mixing.

Proof. It is obvious that strong transitivity implies transitivity. On the other hand, the opposite is also true in this case, as f is piece-wise continuous piece-wise strictly (see Theorem A.4). However, an expanding Lorenz map is transitive if and only if it is chaotic in the sense of Devaney (see e.g. Proposition 5 in [6] and references therein). The second part of Theorem A.8 follows from Theorems 4.5, 4.6, 4.7, 4.8 in [50] and above observations (see also Theorem 7 in [6]). □

Corollary A.9. *An expanding Lorenz-map $f : [0,1] \to [0,1]$ is chaotic in the sense of Devaney (on $[0,1]$) if and only if it has a dense orbit.*

Proof. It is easy to justify that the existence of a dense orbit implies transitivity. The opposite implication holds for Lorenz-like maps (not necessarily expanding) in the view of Proposition 1 in [52]. Now the equivalence with chaos in the sense of Devaney for expanding Lorenz maps follows from Theorem A.8. □

Appendix B. Proof of Theorem 1.5

Proof of Theorem 1.5. Firstly, let us assume that f is strictly increasing in each of the continuity intervals $[0,c)$ and $(c,1]$. Suppose that (7) holds and consider $g\colon [0,1] \to [0,1]$ defined as $g(x) = f^2(x)$. Then g has precisely three discontinuity points c_1, c and c_2 such that $0 < c_1 \in f^{-1}(c) \cap (0,c)$ and $c < c_2 \in f^{-1}(c) \cap (c,1)$. Let us investigate the limits of g at these discontinuity points. We have:

$$\lim_{x \to c_1^-} g(x) = \lim_{x \to c_2^-} g(x) = 1$$
$$\lim_{x \to c_1^+} g(x) = \lim_{x \to c_2^+} g(x) = 0$$
$$\lim_{x \to c^-} g(x) = f(1), \quad \lim_{x \to c^+} g(x) = f(0).$$

Between the discontinuity points the graph of g is continuous and increasing. Thus by analyzing these limits, we see that g has (at least) two-fixed points: $x_1 \in (c_1, c)$ and $x_2 \in (c, c_2)$. On the other hand, f cannot have fixed points in the intervals (c_1, c) and (c, c_2). Indeed, suppose that $x_* \in (c_1, c)$ is a fixed point of f, i.e. $f(x_*) = x_*$. Then $f(c_1) = c$ since $c_1 \in f^{-1}(c)$. As f is increasing, we have $f(c_1) < f(x_*)$ which means $c < x_*$, contradicting the assumption that $x_* \in (c_1, c)$. Similarly, f cannot have fixed points in (c, c_2). Thus the points x_1 and x_2 are not fixed points and must be points of period 2 and we have proved the existence of period 2 periodic orbit.

The above reasoning also applies if f is not strictly increasing in its continuity intervals but is strictly increasing at all those arguments x such that $f(x) = c$. Now, let us see what changes

MOST WIEDZY Downloaded from mostwiedzy.pl

if there are intervals $[c_{1,1}, c_{1,2}] \subset (0, c)$ and/or $[c_{2,1}, c_{2,2}] \subset (c, 1)$ such that $f(x) = c$ for each $x \in [c_{1,1}, c_{1,2}] \cup [c_{2,1}, c_{2,2}]$. Then for the map $g = f^2$ we have

$$\lim_{x \to c_{1,1}^-} g(x) = \lim_{x \to c_{2,1}^-} g(x) = 1$$
$$\lim_{x \to c_{1,2}^+} g(x) = \lim_{x \to c_{2,2}^+} g(x) = 0$$

and $g(x) = f(c) = 0$ for $x \in [c_{1,1}, c_{1,2}] \cup [c_{2,1}, c_{2,2}]$. Similarly, as before g has at least two fixed points: $x_1 \in (c_{1,2}, c)$ and $x_2 \in (c, c_{2,1})$, which simultaneously cannot be fixed points of f since f cannot have fixed points in these intervals. Thus x_1 and x_2 are period 2 periodic points.

For the expanding case, uniqueness of this orbit, as a period 2 periodic orbit, follows from the forthcoming Proposition F.8. The fact that it is unstable is also an immediate consequence of the expansiveness. □

Remark B.1. It is worth pointing out that there is also a natural geometric method for both justification of Theorem 1.5 and graphical locating of 2-periodic points. Namely, let us consider the square $S = [0, 1] \times [0, 1]$ on the plane and the two curves in S: $\gamma_1 \colon [0, c] \to S$ given by $\gamma_1(t) = (t, f(t))$ (assume for simplicity that $\gamma_1(c) = (c, 1)$) and $\gamma_2 \colon [c, 1] \to S$ given by $\gamma_2(t) = (f(t), t)$. Observe that the curve γ_1 is a part of the plot of f (between 0 and c) and the curve γ_2 is the reflection of the other part of the plot of f (between c and 1) in axial symmetry with respect to the diagonal of the square. Moreover, the points of intersection of these curves correspond exactly to 2-periodic points for f. Namely, if there are $t_1 \in [0, c)$ and $t_1 \in [0, c)$ such that $\gamma_1(t_1) = \gamma_2(t_2)$, then $t_1 = f(t_2)$ and $t_2 = f(t_1)$, which gives $t_1 = f^2(t_1)$, i.e., $\{t_1, t_2\}$ is a 2-periodic orbit.

Why do these curves have to intersect? Consider four points on the boundary of S: $A = \gamma_1(0) = (0, f(0))$, $B = \gamma_1(c) = (c, 1)$, $A = \gamma_2(c) = (0, c)$ and $A = \gamma_2(1) = (f(1), 1)$. By the assumption $f(0) < c < f(1)$, C is above A on the left side of the square S and B is to the left of D on the upper side of the square. Hence the curves γ_1 and γ_2 have to intersect at least once from Jordan Curve Theorem (see Figure 22). Finally, if f is an expanding Lorenz map, then the slope of γ_1 at each point is greater than 1 and the slope of γ_2 at each point is less than 1. In consequence, the curves cannot intersect more than once.

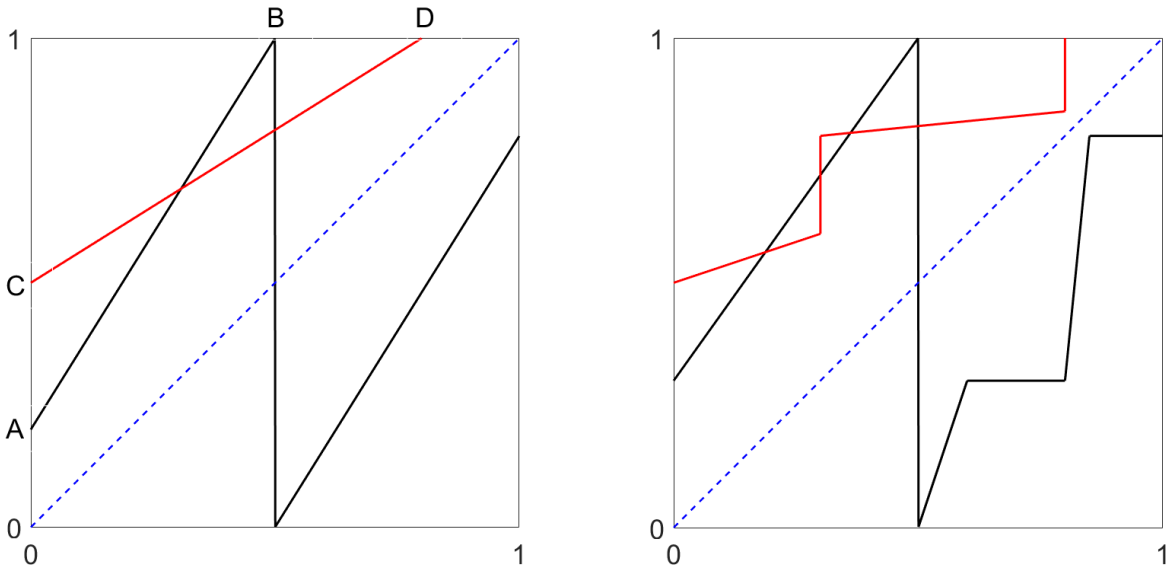

FIGURE 22. Geometric method for finding 2-periodic points. Expanding Lorenz map with a unique 2-periodic point (left) and Lorenz-like map with 3 such points (right).

MOST WIEDZY Downloaded from mostwiedzy.pl

Appendix C. Proof of Theorem 3.2

Proof of Theorem 3.2. Note that five curves go through the point $(F(d), 0)$ in the α-β plane (see Table 1 and Figure 23). Namely, the vertical line $\alpha = F(d)$, the horizontal line $\beta = 0$, the slant line $\beta = F(d) - \alpha$ and two nonlinear curves: $\beta = p(\alpha) = F(d + F(d) - \alpha) - \alpha$ and $\beta = q(\alpha)$. The last one given by the implicit formula

$$L(\alpha, \beta) = F(d + F(d) - \alpha - \beta) - \alpha = 0.$$

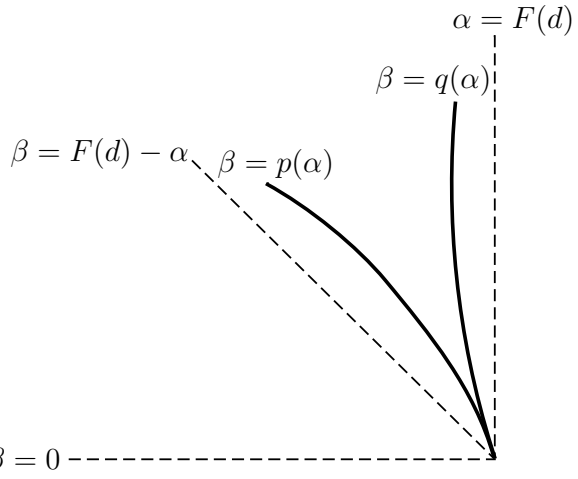

Figure 23. Five curves from the proof of Theorem 3.2.

Since, by our assumptions, the area (parallelogram) between lines $\alpha = F(d + F(d) - \alpha - \beta)$, $\alpha = F(d)$, $\beta = F(d) - \alpha$ and $\beta = d + F(d) - x_{\min} - \alpha$ is always nonempty and the plot of $\beta = p(\alpha)$ is above the line $\beta = F(d) - \alpha$ for $\alpha < F(d)$ (compare the derivatives at $\alpha = F(d)$), to complete the proof it is enough to show that in the small neighbourhood of the point $\alpha = F(d)$ the plot of of $\beta = q(\alpha)$ is above the plot $\beta = p(\alpha)$, which is equivalent to $p'(\alpha) > q'(\alpha)$ (see Figure 23 and compare the slopes of $p(\alpha)$ and $q(\alpha)$ at $\alpha = F(d)$). An easy computation gives

- $p'(\alpha) = -F'(d + F(d) - \alpha - \beta) - 1$ and $p'(F(d)) = -F'(d) - 1$,
- $q'(\alpha) = -\dfrac{\partial L}{\partial \alpha} \Big/ \dfrac{\partial L}{\partial \beta} = \dfrac{-F'(d + F(d) - \alpha - \beta) - 1}{F'(d + F(d) - \alpha - \beta)}$ and $q'(F(d)) = \dfrac{-F'(d) - 1}{F'(d)}$.

Hence, finally, $p'(\alpha) > q'(\alpha)$ if and only if $F'(d) < 1$, which completes the proof. □

Appendix D. Proof of Theorem 4.3

Proof of Theorem 4.3. Note that due to Theorem 4.1 (i) it is enough to show that under Assumption (10) inside the area A there is a nonempty subarea C on which

$$\sqrt{2} \le \lambda = \inf \{G'(x) \mid x \in [b, c]\} \le 2.$$

It is easy to check that the condition $\lambda \le 2$ is satisfied even without Assumption (10). Namely, since $a \in (0, 1)$, $\mu \in (0, 3]$ and $G'(x) = -3\mu x^2 + 2\mu(a + 1)x + 1 - \mu a$ attains maximum at $\frac{a+1}{2}$, we have

$$\lambda \le \sup \{G'(x) \mid x \in [b, c]\} = \frac{\mu(a^2 - a + 1) + 3}{3} \le \frac{3 \cdot 1 + 3}{3} = 2.$$

Now let us check when the condition $\lambda \ge \sqrt{2}$ is satisfied. Observe that λ obviously depends on α and β, because we calculate λ on $[b, c]$. Recall that in Section 3 we searched for invariant intervals inside the interval $(x_{\min}, x_{\max})$ defined by the condition $\lambda > 1$. Now we want to strengthen our condition to $\lambda \ge \sqrt{2}$ and see when parameters α and β for which this condition holds exist. It turns out that this is the case exactly if

- the quadratic equation $G'(x) = \sqrt{2}$ has two distinct real roots or, equivalently as we have seen, $\mu > 3(\sqrt{2} - 1)/(a^2 - a + 1)$,

MOST WIEDZY Downloaded from mostwiedzy.pl

- the endpoints of the invariant interval lie inside the interval (x_1, x_2), i.e., $x_1 < b < c < x_2$.

TABLE 5. Conditions for the existence of chaos.

No.	Condition	Parametric form
7.	$\Delta > 0$	$\mu > 3(\sqrt{2}-1)/(a^2-a+1)$
8.	$x_1 < b$	$d + F(d) - x_1 - \alpha - \beta > 0$
9.	$x_2 > c$	$d + F(d) - x_2 - \alpha < 0$

However, since the discontinuity point d lies in the interval (x_1, x_2), i.e., $x_1 < d < x_2$, the straight line $\beta = d+F(d)-x_1-\alpha$ is parallely above $\beta = d+F(d)-x_1-\alpha$ and the vertical line $\alpha = d+F(d)-x_2$ is on the left of $\alpha = F(d)$ (see Figure 4). In consequence, if (10) holds, then the conditions 8. and 9. from Table 5 always cut by rectilinear cuts from the area A the subarea of positive Lebesgue measure. Since this subarea is obviously contained in C, the proof is complete. □

APPENDIX E. PROOF OF THEOREM 5.2

Proof of Theorem 5.2. The reasoning is similar to that in the proof of Theorem 3.2. Let us consider four nonlinear curves (see Figure 24), which intersect at the point $\alpha = \alpha_0 = F(d)$. Two of them $\beta = p(\alpha)$ and $\beta = p(\alpha)$ correspond to the borders of the set A (see the proof of Theorem 3.2). The other two $\beta = r(\alpha)$ and $\beta = s(\alpha)$ correspond to the borders of the set B. Namely, $\beta = r(\alpha)$ is given by the implicit formula $F(d+F(d)-\alpha-\beta)+F(d)-2\alpha-\beta = 0$, which corresponds to the condition 10. (see Table 2), and $\beta = s(\alpha)$ is given by the explicit formula $\beta = F(d + F(d) - \alpha) + F(d) - 2\alpha$, which corresponds to the condition 11. Since all four curves are smooth and have a common point $(\alpha_0, 0)$, the proof will be completed by showing that the derivatives at α_0 satisfy the following three conditions: (a) $r'(\alpha_0) > s'(\alpha_0)$, (b) $r'(\alpha_0) > q'(\alpha_0)$ and (c) $p'(\alpha_0) > s'(\alpha_0)$.

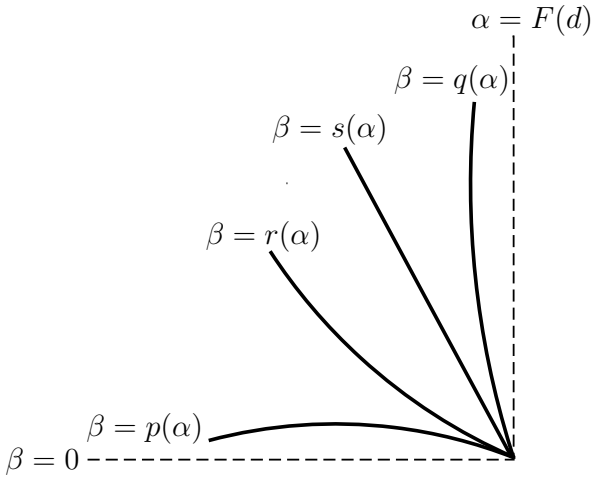

FIGURE 24. Four nonlinear curves from the proof of Theorem 5.2.

Note that we do not assume any relations between $s'(\alpha_0)$ and $q'(\alpha_0)$ and between $r'(\alpha_0)$ and $p'(\alpha_0)$. For abbreviation, let ζ stands for $F'(d)$. An easy calculation similar to that in the proof of Theorem 3.2 shows that

$p'(\alpha_0)$	$q'(\alpha_0)$	$r'(\alpha_0)$	$s'(\alpha_0)$
$-\zeta - 1$	$\frac{-\zeta-1}{\zeta}$	$\frac{-\zeta-2}{\zeta+1}$	$-\zeta - 2$

Now, since $\zeta = F'(d) > 0$, we check at once that the conditions (a), (b) and (c) are satisfied, which completes the proof. □

MOST WIEDZY Downloaded from mostwiedzy.pl

Appendix F. Finite unions of periodic orbits and Farey–Lorenz permutations

Let f be a Lorenz-like map. If $P := \{x, f(x), \dots, f^{q-1}(x)\}$ is a periodic orbit of f, then the itinerary of P is the sequence $(a_1, a_2, \dots, a_q)$ of symbols L and R such that for $i = 1, \dots, q$

$$a_i = \begin{cases} L, & \text{if } f^i(x) \in I_L \\ R, & \text{if } f^i(x) \in I_R \end{cases}.$$

The sequence is given up to a cyclic permutation.

Definition F.1. A **f**inite **u**nion of **p**eriodic **o**rbits of f is called a *fupo*.

Fupos are characterized by their permutations, i.e., a permutation of a fupo P consisting of points $x_1 < \cdots < x_n$, is a mapping $\sigma : \{1, 2, \cdots, n\} \to \{1, 2, \cdots, n\}$ such that $f(x_i) = x_{\sigma(i)}$.

The following observation applies to fupos of Lorenz-like maps.

Proposition F.2. *If a fupo P has $n > 1$ elements, then there exists $k \in \{1, \dots, n-1\}$ such that σ is increasing on $\{1, \dots, k\}$ and on $\{k+1, \dots, n\}$. Such permutations (and the permutation of $\{1\}$) are called* L-permutations*. Moreover, for every L-permutation σ there exists a Lorenz-like map f with the fupo P such that P has permutation σ.*

Note that is fupo is a periodic orbit, then its rotation number is $(n-k)/n$.

Definition F.3. A cyclic L-permutation σ of $\{1, \dots, n\}$ is called a *twist* permutation if $\sigma(1) > \sigma(n)$.

Correspondingly, a periodic orbit with such a permutation is called a *twist* periodic orbit.

Remark F.4. Note that a twist permutation of $\{1, \dots, n\}$ with rotation number j/n has a form

$$\sigma(i) = i + j \mod n.$$

In consequence, the kth term of the twist periodic itinerary is L if and only $(kp \mod q) < q - p$.

Definition F.5. An L-permutation σ of $\{1, \dots, p+q\}$ is called a *Farey–Lorenz permutation* (or *FL-permutation*) if σ consists of two twist cycles, of period p and q, with rotation numbers $a/p < b/q$ respectively, such that $bp = aq + 1$.

Recall that in this case we say that a/p and b/q are *Farey neighbours*. The ordering of point on fupos with FL permutations are specified by the following rule (cf. [23]).

Proposition F.6. *Assume that σ is an FL-permutation with cycles of rotation numbers a/p and b/q, where $a/p < b/q$ are Farey neighbours and $p < q$. Let the points of P be $x_1 < x_2 < \cdots < x_p$ and the points of Q, $y_1 < y_2 < \cdots < y_q$. Then*

$$f(x_i) = x_{i+a \mod p} \quad \text{and} \quad f(y_j) = y_{j+b \mod q}$$

and

- $x_1 < y_1$,
- *for $i = 1, \dots, p-1$, if $j = 1 + ia \mod p$ and $l = ib \mod q$, then $y_{l-1} < x_j < y_l$.*

An example of a fupo of FL type in the 1D nlCNV model is illustrated in Figure 11.

The following result (see e.g. [2] or [23, Sec. 5]) states that Lorenz-like maps admit twist periodic orbits for each rational number in their rotation interval.

Theorem F.7. *Let g be a Lorenz-like map. If a number p/q is in the rotation interval of g, and p, q are coprime, then g has a twist periodic orbit of period q and rotation number p/q.*

If the map is also expanding then we obtain the uniqueness of periodic orbits with given itinerary (see [6, Prop. 1]) for justification).

Proposition F.8. *If g is an expanding Lorenz map and p/q is in the rotation interval of g (p and q coprime) then there is exactly one twist periodic orbit with rotation number p/q. Moreover, there is at most $\binom{q}{p}/q$ periodic orbits with with rotation number p/q.*

MOST WIEDZY Downloaded from mostwiedzy.pl

Remark F.9. In fact, we show in [6] that given any periodic *L-R* sequence there is at most one periodic orbit with this itinerary.

Next theorem, proved in [23], applies for Lorenz-like maps (not necessarily expanding).

Theorem F.10. *Let g be a Lorenz-like map. Assume that the rotation interval of g contains the interval $[a/p, b/q]$, where $a/p < b/q$ are Farey neighbours, and $p < q$. Then g has a twist periodic P orbit of period p and rotation number a/p and a twist periodic orbit Q of period q and rotation number b/q. If these periodic orbits are disjoint, then their union forms a fupo with the FL-permutation. Moreover, there exist periodic orbits with itineraries being concatenation of finitely many periodic itineraries (starting at x_1 or y_1) of P and Q.*

Remark F.11. If $a/p < b/q$, but $p > q$, then we replace a/p by $(p-a)/p$ and b/q by $(q-b)/q$. Then, in the itineraries we replace symbols L by R and vice versa.

MOST WIEDZY Downloaded from mostwiedzy.pl